Structural Characterization of an *N*-Acetyl-2-aminofluorene (AAF) Modified DNA Oligomer by NMR, Energy Minimization, and Molecular Dynamics†

Suzanne F. O'Handley,‡ David G. Sanford,‡ Rong Xu,§ Cathy C. Lester,‡ Brian E. Hingerty,‖ Suse Broyde,⊥ and Thomas R. Krugh*,‡

Department of Chemistry, University of Rochester, Rochester, New York 14627, Department of Chemistry, New York University, New York, New York 10003, Health and Safety Research Division, Oak Ridge National Laboratory, Oak Ridge, Tennesee 37831, and Department of Biology, New York University, New York, New York 10003

Received August 31, 1992; Revised Manuscript Received December 7, 1992

ABSTRACT: An *N*-acetyl-2-aminofluorene (AAF) modified deoxyoligonucleotide duplex, d(C1-C2-A3-C4-[AAF-G5]-C6-A7-C8-C9)·d(G10-G11-T12-G13-C14-G15-T16-G17-G18), was studied by one- and two-dimensional NMR spectroscopy. Eight of the nine complementary nucleotides form Watson–Crick base pairs, as shown by NOEs between the guanine imino proton and cytosine amino protons for G·C base pairs or by an NOE between the thymine imino proton and adenine H2 proton for A·T base pairs. The AAF-G5 and C14 bases show no evidence of complementary hydrogen bond formation to each other. The AAF-G5 base adopts a syn conformation, as indicated by NOEs between the G5 imino proton and the A3–H3′ and A3–H2′/H2″ protons and by NOEs between the fluorene-H1 proton of AAF and the G5-H1′ or C6-H1′ proton. The NOEs from the C4-H6 proton to C4 sugar protons are weak, and thus the glycosidic torsion angle in this nucleotide is not well defined by these NMR data. The remaining bases are in the anti conformation, as depicted by the relative magnitude of the H8/H6 to H2′ NOEs when compared to the H8/H6 to H1′ NOEs. The three base pairs on each end of the duplex exhibit NOEs characteristic of right-handed B-form DNA. Distance restraints obtained from NOESY data recorded at 32 °C using a 100-ms mixing time were used in conformational searches by molecular mechanics energy minimization studies. The final, unrestrained, minimum-energy conformation was then used as input for an unrestrained molecular dynamics simulation. Chemical exchange cross peaks are observed, and thus the AAF-9-mer exists in more than a single conformation on the NMR time scale. The NMR data, however, indicate the presence of a predominant conformation (≥70%). The structure of the predominant conformation of the AAF-9-mer shows stacking of the fluorene moiety on an adjacent base pair, exhibiting features of the base-displacement [Grunberger, D., Nelson, J. H., et al. (1970) *Proc. Natl. Acad. Sci. U.S.A. 66*, 488–494] and insertion-denaturation models [Fuchs, R. P. P., & Daune, M. (1971) *FEBS Lett. 14*, 206–208], while the distal ring of the fluorene moiety protrudes into the minor groove.

N-Acetoxy-2-acetylaminofluorene, AAAF, a member of a class of tumorigenic aromatic amines, has been widely studied as a model chemical carcinogen (Kriek, 1969; Basu & Essigmann, 1988; Beland & Kadlubar, 1990). AAAF reacts with single-stranded DNA in vitro with a high degree of specificity for the C^8 position of guanine, forming the *N*-(deoxyguanosin-8-yl)-2-(acetylamino)fluorene adduct, AAF-G. The acetyl group on the AAF-G adduct (shown in Figure 1) is too bulky to fit into the crowded region near its own sugar when the modified guanine is in the anti domain of B-form DNA. This steric problem can be alleviated by rotation of the guanine to a syn conformation, as suggested in the base displacement model of Grunberger et al. (1970), and the insertion-denaturation model of Fuchs and Daune (1971, 1972). The proposed syn guanine orientation of the AAF-G base is in accord with early NMR studies of modified nucleosides (Evans et al., 1980) and CD and NMR studies of monomers and dimers [e.g., Nelson et al. (1971) and Leng et al. (1980)]. Furthermore, AAAF reaction with alternating G–C sequence DNAs promotes the B–Z transition (Sage & Leng, 1980; Santella et al., 1981a,b) in which the AAF-modified guanine adopts a syn conformation (Wang et al., 1979), with the 2-(acetylamino)fluorene located outside of the helix (Sage & Leng, 1980; Santella et al., 1981a,b). The

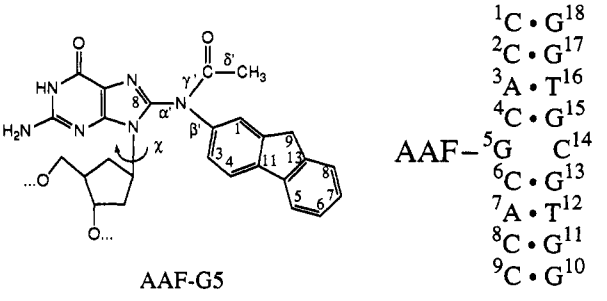

FIGURE 1: Chemical structure of *N*-(deoxyguanosin-8-yl)-*N*-(2-acetylamino)fluorene, AAF-G5, and the schematic for the AAF-modified 9-mer duplex. The dihedral angles A–B–C–D are defined as follows: χ(pur), O1′–C1′–N9–C4; α′, N9–C8–N–C2; β′, C8–N–C2–C1; γ′, C8–N–C–C_m; δ′, N–C–C_m–H (C_m is the methyl carbon of the acetyl group). The angle A–B–C–D is measured by a clockwise rotation of D with respect to A, looking down the B–C bond; A eclipsing D is 0°.

† This publication was supported in part by Grants CA35251 (T.R.K.) and CA28038 (S.B.) from the National Cancer Institute, DOE Grants DE-FG02-91ER60931 (S.B.) and DE-AC05-840R21400 with Martin Marietta Energy Systems (B.E.H.); NSF Grant DMB 8611927 (T.R.K.), and NIH Grants RR03317 (T.R.K.) and RR06458 (S.B.). Calculations were performed on the Cray supercomputers at the DOE National Energy Research Supercomputer Center and at the National Science Foundation San Diego Supercomputer Center. The contents of this paper are solely the responsibility of the authors and do not necessarily represent the official views of the funding agencies.

‡ Department of Chemistry, University of Rochester.
§ Department of Chemistry, New York University.
‖ Oak Ridge National Laboratory.
⊥ Department of Biology, New York University.

0006-2960/93/0432-2481$04.00/0

large number of early experimental studies are reviewed in Singer and Grunberger (1983). In recent experiments, Fuchs and co-workers used chemical probes (Belguise-Valladier & Fuchs, 1991) and DNA footprinting (Veaute & Fuchs, 1991) to characterize structural polymorphism evident in AAF mutation spectra (Lambert et al., 1992); their data suggest strongly that the local structure surrounding the adduct will depend upon the sequence at the site where the AAF is attached.

More recent NMR studies have investigated structural aspects of AAF adducts with mononucleotides (Evans & Levine, 1987), dinucleotides (Evans & Levine, 1988), and a hexanucleotide at the single-strand level (Sharma & Box, 1985). Patel and co-workers (Norman et al., 1989) have used two-dimensional NMR and molecular mechanical calculations to determine the solution structure of a DNA 11-mer modified at a central guanine by the related aromatic amine 2-aminofluorene (AF), with adenine opposite the modified G. In this structure the AF-G adopts a syn conformation while its opposite adenine is in the anti form. The AF is buried snugly within the wall of the minor groove. The G opposite A mispairing represents the view following mutagenic replication in which the predominant G·C → T·A transversion has occurred (Bichara & Fuchs, 1985; Basu & Essigmann, 1988).

Early computational investigations also showed that the syn domain of AAF-modified guanosine is overwhelmingly preferred over the anti conformation (Lipkowitz et al., 1982) and that AAF–base stacking is an important structural feature in the modified deoxydinucleoside monophosphate, d(CpG) (Hingerty & Broyde, 1982a). More recent computational investigations (Shapiro et al., 1989) incorporating AAF-G with syn guanine into B-DNA produced a number of models, differing in extent of helix insertion versus protrusion of the fluorene rings into the minor groove. In addition, a model has been presented which depicts an AAF induced frameshift mutation; the -2 deletion is achieved by rotation of the modified guanine to syn and insertion of the AAF into the helix, with attendant misalignment of the partner strand (Broyde & Hingerty, 1987; Broyde et al., 1990). An in vacuo molecular dynamics simulation using AMBER of an AAF-modified guanosine and AAF-modified Z-DNA has been presented by Fritsch and Westhof (1991). The use of molecular dynamics simulations to characterize DNA oligomers is reviewed by Beveridge et al. (1993).

We report the structure of an AAF-G adduct incorporated into a DNA 9-mer duplex in which the AAF-G adduct is positioned opposite a complementary base, cytosine, giving an AAF-G[syn]–C[anti] alignment. The lesion is incorporated into an AAF-modified DNA 9-mer d(C1-C2-A3-C4-[AAF-G5]-C6-A7-C8-C9)·d(G10-G11-T12-G13-C14-G15-T16-G17-G18). We refer to this duplex as the AAF-9-mer. Preliminary studies (Sanford & Krugh, 1985) and the present data show that the AAF-9-mer is of sufficient length to provide a stable duplex. Optical experiments on AAF-modified d(TACGTA) (Sharma & Box, 1985) and the AAF-9-mer (Sanford & Krugh, 1985) showed marked changes in CD spectra upon adduct formation, with the induction of a negative band in the 280-nm region, suggesting the possible formation of a left-handed duplex. This tentative interpretation of the CD spectra of the AAF-9-mer was misleading because the NMR data show that the AAF-9-mer duplex is primarily right-handed, with the exception of the modified guanine where the AAF-G5 base does adopt a syn conformation. Thermal melting data at 305 nm (Sanford & Krugh, 1985) suggested the possibility of stacking between the fluorene moiety and adjacent bases. The present data, and the preliminary description of these results (O'Handley et al., 1992), show stacking of the AAF moiety on G15, with the modified guanine displaced from the duplex and located in the major groove. The structure of the AAF-9-mer is reminiscent of features of the base-displacement (Grunberger et al., 1970) and insertion-denaturation models (Fuchs & Daune, 1971, 1972); protrusion of the fluorene out into the minor groove is also a significant feature.

The analysis of the two-dimensional NMR data for the AAF-9-mer was complicated by the presence of chemical exchange cross peaks for some of the resonances. Although more than one structure is present in slow exchange on the NMR time scale, one structure predominates (≥70%), and in this paper we focus on the structure of the predominant form of the AAF-9-mer. The structure reported here serves as a model for adducts of AAF with DNA prior to replication where the modified guanine has its normal partner. This structure, therefore, may be helpful in visualizing relevant conformations important in both replication and repair processes.

MATERIALS AND METHODS

Materials. *N*-Acetoxy-2-acetylaminofluorene, AAAF, was purchased from the National Cancer Institute repository operated by Midwest Research Institute. The oligodeoxynucleotides d(CCACGCACC) and d(GGTGCGTGG) were synthesized by the phosphoramidite method on an Applied Biosystems synthesizer in Dr. George Levy's laboratory at Syracuse University, Syracuse, NY.

Purification of Oligonucleotides. Ammonialysis was performed for 12 h at 55 °C to cleave the protecting groups. The dimethoxytrytl (DMT) bearing oligomers were separated from failure sequences using reverse-phase HPLC on a PRP-1 column from Hamilton (Huang & Krugh, 1990). The mobile phase consisted of buffer A (0.01 M potassium phosphate, pH 7) and buffer B (70% acetonitrile, 10% methanol, 20% buffer A). A solvent of 85% buffer A/15% buffer B was run for 5 min followed by a 40-min gradient from 85% buffer A/15% buffer B to 45% buffer A/55% buffer B. After isolation of the desired DMT-bearing oligomers, cleavage of the DMT group was accomplished by reaction with 80% acetic acid for 20 min at room temperature. Ethanol and water were then added to facilitate evaporation of the acetic acid upon drying. After removal of the acid, the DMT group was extracted with ether. Sep-Pak cartridges (Waters) were used to desalt the oligomers.

Modification of Oligonucleotides with AAAF. The d(CCACGCACC) oligomer was dissolved in 0.002 M sodium citrate buffer to give a DNA concentration of approximately 2 mM. AAAF was dissolved in sufficient ethanol to yield 13% ethanol by volume when added to the oligomer solution. The oligomer solution was purged with nitrogen. AAAF was added to give an 8:1 ratio of carcinogen to DNA, and the reaction mixture was shaken at 37 °C for 3 h. Undissolved AAAF went into solution as the reaction progressed. Excess AAAF was extracted with ether. The d(CCAC[AAF-G]CACC) was separated from unmodified oligomer and minor adducts via reverse-phase HPLC on a PRP-1 column. The mobile phase gradient was 95% buffer A/5% buffer B to 65% buffer A/35% buffer B in 30 min. The final reaction yield was approximately 70%. The isolated d(CCAC[AAF-G]CACC) solution was concentrated on a Savant Speed-Vac concentrator and desalted on Waters Sep-Pak cartridges.

Duplex Formation. Proton NMR spectroscopy was used to determine the appropriate volumes of the solutions containing d(CCAC[AAF-G]CACC) and d(GGTGCGTGG) needed to give a 1:1 ratio of the two strands. The disappearance of single-strand resonances and appearance of duplex resonances was used as a monitor of duplex formation to determine the concentrations required (O'Handley, 1991).

Sample Preparation. All samples were put through a Chelex column prior to NMR experiments. The final buffer solution contained 0.1 M sodium chloride, 10 mM sodium phosphate, and 0.5 mM EDTA and was adjusted to the proper pH with NaOH or HCl. The sample concentration was 7.6 mM duplex in 300 μL for the 450-ms NOESY experiment and the DQCOSY experiment and 4.6 mM in 500 μL for the remaining experiments. Experiments were performed in either D_2O or 90:10 H_2O/D_2O (v/v). Samples in D_2O were lyophilized and exchanged with D_2O three times. NMR experiments were recorded with samples at pH 6.0, 7.0, and 8.5.

NMR Experiments. All NMR experiments were performed on a 500-MHz Varian VXR-500S NMR spectrometer. The majority of experiments were recorded at temperatures between 5 and 32 °C, with most of the assignments made at 32 °C for the nonexchangeable protons and at 6 °C for the exchangeable protons; the temperature of each experiment is indicated in the text and figure legends.

phanoejr. The phanoejr pulse sequence (courtesy of A. Pardi, University of Colorado), a 2D NOESY pulse sequence with a jump-and-return pulse sequence incorporated for solvent suppression, was used to obtain a 2D NOESY spectrum in H_2O solvent at 6 °C. The water resonance was partially saturated for 0.5 s during the relaxation delay with a decoupler power of 35. A sweep width of 12 000 Hz was used in both dimensions, using an offset value of 1330 Hz with a mixing time of 130 ms. A total of 4K data points were collected in the t_2 dimension, 256 complex t_1 values were collected for each data set, and 96 transients were collected for each t_1 value. The data were apodized with shifted sine bell functions in both dimensions (sb = –0.170, sbs = –0.169, sb1 = –0.017, sbs1 = –0.016) and zero filled in t_1 to give a 4K by 1K data matrix.

NOESY Experiments. Phase-sensitive proton NOESY experiments were recorded in D_2O solution with sweep widths of approximately 5000 Hz at temperatures and mixing times as specified in the figure legends. The transmitter frequency was set on the residual HOD resonance, which was presaturated during the 3-s relaxation delay. A steady-state pulse sequence was applied at the beginning of the relaxation delay. A total of 4096 data points were collected in the t_2 dimension, 768 t_1 values were collected for each data set, and 32 transients were collected for each t_1 value. The data were apodized with shifted Gaussian functions in both dimensions (gf = 0.088, gfs = 0.034, gf1 = 0.047, gfs1 = 0.016) and zero filled in t_1 to give a 4K by 2K data matrix. The NOESY spectrum used for structural analysis was recorded at 32 °C and had a mixing time of 100 ms. The transmitter frequency was set on the residual HOD resonance which was presaturated during the 5-s relaxation delay. A total of 2048 complex data points were collected in the f_2 dimension, 256 complex t_1 values were collected for each data set, and 96 transients were collected for each t_1 value. The data were apodized with Gaussian functions in both dimensions (gf = 0.079 and gf1 = 0.019) and zero filled to give a 4K by 2K data matrix.

DQCOSY Experiments. A DQCOSY spectrum was recorded at 32 °C. The transmitter frequency was set on the residual HOD resonance, which was presaturated during the 2-s relaxation delay. A steady-state pulse was also applied during this delay period. A total of 4096 data points were collected in the t_2 dimension, 512 t_1 values were collected for each data set, and 16 transients were collected for each t_1 value. The data were apodized with shifted sine bell functions in both dimensions (sb = –0.208, sbs = –0.177, sb1 = –0.049, sbs1 = –0.018) and zero filled to give a 4K by 2K data matrix.

TOCSY Experiments. TOCSY spectra were recorded at temperatures corresponding to those used for NOESY spectra, using mixing times of 70–150 ms. A sweep width of 5000 Hz was used in both dimensions. The transmitter frequency was set on the residual HOD resonance, which was presaturated during the 3-s relaxation delay. A steady-state pulse was also applied at the beginning of the relaxation delay. A trim pulse of 0.0010 s was used. A total of 4096 data points were collected in the f_2 dimension, 512 t_1 values were collected for each data set, and 32 transients were collected for each t_1 value. The data were apodized with Gaussian functions in both dimensions (gf = 0.042 and gf1 = 0.016) and displayed as a 2K by 1K data matrix.

Computational Studies. Minimized potential energy calculations in torsion angle space were carried out with the torsion angle space molecular mechanics program DUPLEX, which has been described in full detail (Hingerty et al., 1989). DUPLEX uses a potential energy set similar to one developed by Olson and co-workers (Srinivasan & Olson, 1980; Taylor & Olson, 1983). In addition, a hydrogen bond penalty function (Hingerty et al., 1989) is employed in all first stage minimizations to aid the minimizer in locating designated hydrogen-bonded minima of any type, or denatured sites if the function is not implemented at a particular base pair.

To locate minimum energy conformations suggested from experimental NMR data, pseudopotentials (permitting upper and lower bound restraints) are added to the energy, as described previously (Norman et al., 1989; Schlick et al., 1990). Briefly, the following functions are used:

$$F_N = W_N \sum (d - d_N)^2 \quad (1)$$

$$F_{NN} = W_{NN} \sum (d - d_{NN})^2 \quad (2)$$

W_N and W_{NN} are adjustable weights [in the range of 10–30 kcal/(mol·Å^2)], d is the current value of the interproton distance, d_N is a target upper bound, and d_{NN} a target lower bound. Equation 1 is implemented when d is greater than d_N, and equation 2 is implemented when d is less than d_{NN}. All penalty functions are released in the last minimization steps to yield unrestrained final structures that are energy minima.

Bond lengths, bond angles, dihedral angles, and parameters for AAF and its linkage site to C^8 of guanine were the same as those employed in earlier work (Hingerty & Broyde, 1982b) in studies using DUPLEX. Search strategies and building techniques are described under Results.

Molecular Dynamics Simulations. Molecular dynamics simulations (MDS) with full implementation of solvent and salt were carried out with the program AMBER, version 3.1 (Singh et al., 1988). The starting conformations of both unmodified and modified 9-mer duplexes for the MDS were computed with DUPLEX, as described under Results. The "all atom" representation was used. Parameters for the carcinogen and linkage site were assigned from standard values in the AMBER force field, where available (Weiner et al., 1984; 1986). Those parameters that are not in the standard AMBER set were assigned values that are given in Table S1

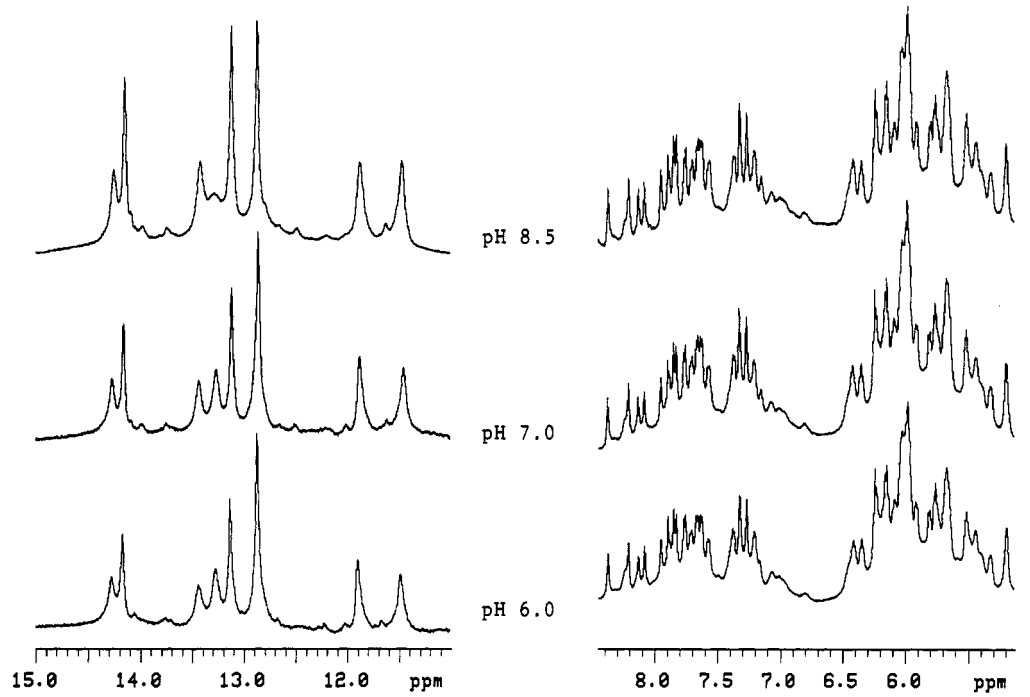

FIGURE 2: Imino proton region (recorded at 6 °C) and the base/H1′ proton region (recorded at 32 °C) of ^{1}H NMR spectra of the AAF-modified 9-mer duplex recorded at pH 6.0, 7.0, and 8.5.

(in the Supplementary Material, ordering information is given on any current masthead page). The electrostatic charges for the carcinogen were calculated using the modified version of Gaussian 80 (Singh & Kollman, 1984), in which quantum mechanically derived electrostatic potentials are fitted to a point charge model. These partial charges, which are consistent with the rest of the AMBER set, are given in Figure A in the Supplementary Material. Phosphates were neutralized with sodium ions by placing them 3.5 Å from the phosphate bisector. The AAF-9-mer was placed in the center of a rectangular box surrounded by repeating cubes of TIP3P·H_2O (Jorgensen et al., 1983). Solvent molecules that were closer than 3.6 Å to any solute atom were removed. The size of the box was such that no DNA atom was closer than 11 Å to any side. Water molecules outside of the rectangular box were removed. A dielectric constant of 1 was employed. The number of water molecules and box dimensions for each of the simulations carried out with these periodic boundary conditions is given in Table S2. The Na^+ concentrations in these boxes range from 0.21 to 0.24 M, appropriate for B-DNA. Each system was first subject to potential energy minimization with AMBER, in 2 steps: in step 1, water molecules alone were minimized, holding DNA rigid; in step 2, the whole system was minimized. This procedure was adopted to allow local ordering of water with no distortion to the starting conformer (Hausheer et al., 1989). In each step, 80 cycles of initial steepest descent minimization were followed by 920 cycles of conjugate gradient minimization. The dynamics simulation was started by assigning a random velocity to each atom in the system so that the velocity distribution conformed to a Maxwellian distribution corresponding to 10 K. Then the system was heated to 298.16 K with a temperature coupling time of 0.1 ps and allowed to equilibrate for 8 ps. The resultant system was then allowed to evolve. The SHAKE routine (van Gunsteren & Berendsen, 1977), in which all bond lengths are held constant, with a tolerance of 0.0005 Å, was used to achieve a time step of 0.002 ps in the MDS. During the simulation, the NMR-derived distances were not used as constraints in the MDS, to allow maximum freedom of motion, as well as to minimize the impact of chemical exchange averaging on the calculated structure. The temperature was held constant at 298.17 K, and the pressure was allowed to fluctuate around 1 bar with a pressure coupling time of 0.6 ps. A nonbonded cutoff of 8.0 Å was used. Coordinate sets were written every 0.1 ps. Improper torsion angle constraints shown in Table S1 were employed for the fluorene ring.

Table I: Chemical Shifts of the Exchangeable Protons in d(CCAC[AAF-G]CACC)·d(GGTGCGTGG)[a]

base pairs	G-N1H	T-N3H	C-N4H$_b$[b]	C-N4H$_{nb}$[b]	G-N2H
C1·G18	13.24		7.96	7.02	
C2·G17	13.10		8.58	7.06	
A3·T16		14.25			
C4·G15	11.45		8.10	6.96	
G5	11.88				6.90
C6·G13	13.40		8.52	7.34	
A7·T12		14.15			
C8·G11	12.85		8.40	6.87	
C9·G10	12.85		8.28	7.09	

[a] The data were recorded at 6 °C for a 4.6 mM sample; values given are in parts per million referenced to the water resonance at 4.98 ppm. [b] C-N4H$_b$ refers to the hydrogen-bonded amino proton. C-N4H$_{nb}$ refers to the non-hydrogen-bonded amino proton.

Calculation of NOESY Spectra. The NOESY spectrum corresponding to a particular structure was calculated with the software package NMR2/MODEL purchased from NMRi Inc. (Syracuse, NY). Exchangeable protons were excluded from the calculations by altering the input structure files so that imino, amino, and terminal OH protons were not considered. All spectra were calculated with a mixing time of 100 ms and an estimated isotropic rotational correlation time of 3 ns. An external relaxation rate, corresponding to spin–lattice relaxation derived from sources other than intramolecular DNA proton–dipolar interactions, was estimated from the average spin–lattice relaxation rate at 500 MHz to be 0.6 s^{-1}. Interactions between a particular proton and all protons residing within a cut-off distance of 10 Å were included in the calculation, and a Gaussian line width of 30

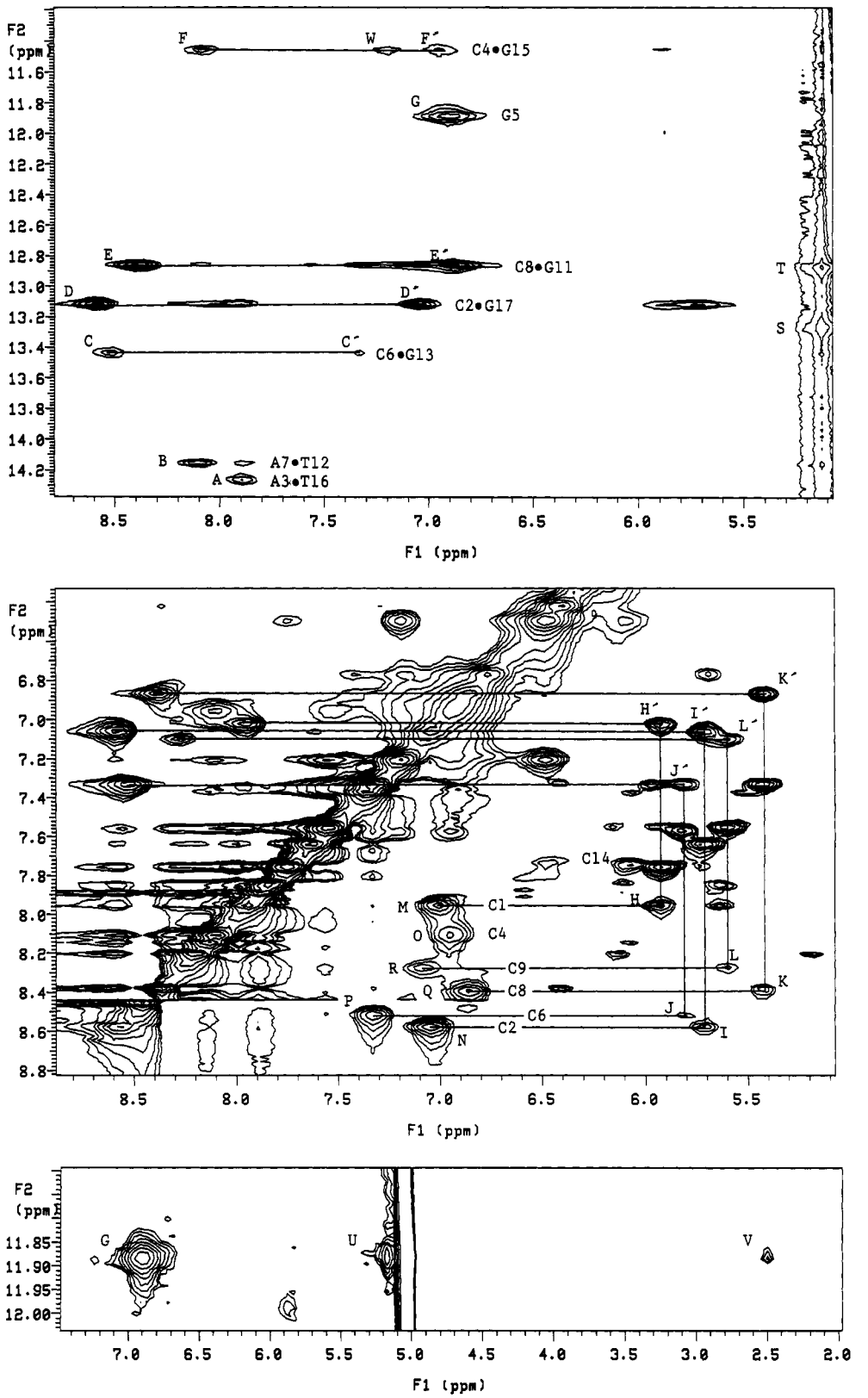

FIGURE 3: Portions of the NOESY spectrum recorded in H_2O at 6 °C with a mixing time of 130 ms used to assign the exchangeable protons. (A, top) Imino to amino region. Cross peaks S and T arise from exchange of the terminal protons with the solvent and are partially obscured by a ridge from the residual solvent. (B, middle) Amino to amino and amino to C-H5 region. (C, bottom) Portion of the NOESY spectrum showing NOEs from the G5 imino proton to A3-H2′/H2″ and A3-H3′.

Hz was used to simulate the cross peaks. The results of the molecular dynamics simulations described above were used to calculate averaged NOESY spectra which were generated by calculating the NOESY spectrum for each structure selected at a specific time point along the molecular dynamics simulation, i.e., every 5 ps, and then computing the average spectrum. An alternative approach in which the intensities of the NOESY cross peaks are calculated from the trajectories of a molecular dynamics simulation has been recently published (Withka et al., 1992).

RESULTS

The downfield portions of the 500 MHz ^{1}H NMR spectra of the AAF-9-mer duplex at pH 6.0, 7.0, and 8.5 are shown in Figure 2. We do not observe any significant differences in these spectra, except for the anticipated broadening of the imino protons of terminal base pairs at pH 8.5 (Figure 2, top). The invariance of the one-dimensional spectra (Figure 2) and two-dimensional NOESY spectra (data not shown) in the pH 6.0–pH 8.5 range in both H_2O and D_2O solvents indicates that the structure of the AAF 9-mer duplex is independent of pH in this range. We would not anticipate a pH dependence of the structure in this pH range unless protonation were facilitated by the formation of a hydrogen bond. The NMR data for the AAF-9-mer used in this study (in which cytosine is opposite the modified guanine) show no indication of protonation or changes in the conformation of the duplex in the pH 6.0–8.0 range.

Assignment of the Exchangeable Protons. Nine imino proton resonances are observed in the one-dimensional spectrum (Figure 2). The imino proton resonances were assigned initially by one-dimensional NOE experiments (G. Huang, D. G. Sanford, and T. R. Krugh, unpublished data). Two-dimensional NOESY experiments performed in H_2O solution at 6 °C (Figure 3) confirmed the assignments of the imino protons and provided the amino proton assignments (Table I).

The A3·T16 imino proton resonance at 14.25 ppm and the A7·T12 imino proton resonance at 14.15 ppm are assigned from NOEs observed between the thymine imino protons and the adenine H2 proton on the complementary base (cross peaks A and B in Figure 3A). The A3-H2 and A7-H2 protons were assigned from base to sugar NOEs; the A3-H2 proton exhibits an NOE to A3-H1′, and the A7-H2 proton has NOEs to A7-H1′ and C8-H1′ (cross peaks a, b, and c in Figure 4A).

The H5 protons of the C1, C2, C6, C8, and C9 bases exhibit NOEs to both the hydrogen-bonded and the non-hydrogen-bonded amino protons (cross peaks H–L and H′–L′ in Figure 3B). The amino protons from each of these cytosines also exhibit an NOE to one another (cross peaks M–R in Figure 3B). NOEs are exhibited for each of the C2, C6, and C8 bases from both cytosine amino protons to the guanine imino proton of the complementary base (cross peaks C–F and C′–F′ in Figure 3A). These connectivities are used to assign the resonances at 13.40, 13.10, and 12.85 ppm to the C6·G13, C2·G17, and C8·G11 imino protons, respectively.

In the present experiment we did not observe an NOE between the amino protons from C1 and C9 to their adjacent imino protons. The C1·G18 and C9·G10 imino protons were identified by exchange cross peaks with water in the NOESY spectrum at 6 °C (cross peaks S and T in Figure 3A). The assignments for the terminal base pairs included in Table I were made by comparison of the chemical shifts for the terminal base pairs in the AAF-9-mer duplex to the unmodified 9-mer duplex (O'Handley and Krugh, unpublished data) and to published spectra for other DNA oligomers containing the same sequences on the 3′ and 5′ ends (Kan et al., 1982; Patel & Shapiro, 1985; Norman et al., 1989).

The resonance at 11.45 ppm belongs to the C4·G15 imino proton, since 1D NOEs indicate that this base pair is adjacent to the A3·T16 base pair (the C2·G17 imino proton on the other side of A3·T16 had been assigned already). The C4·G15 imino proton shows NOEs to both the hydrogen-bonded and non-hydrogen-bonded C4 amino protons (cross peaks F and F′ in Figure 3A), and the C4 amino protons show NOEs to one another (cross peak O in Figure 3B). The C4 amino

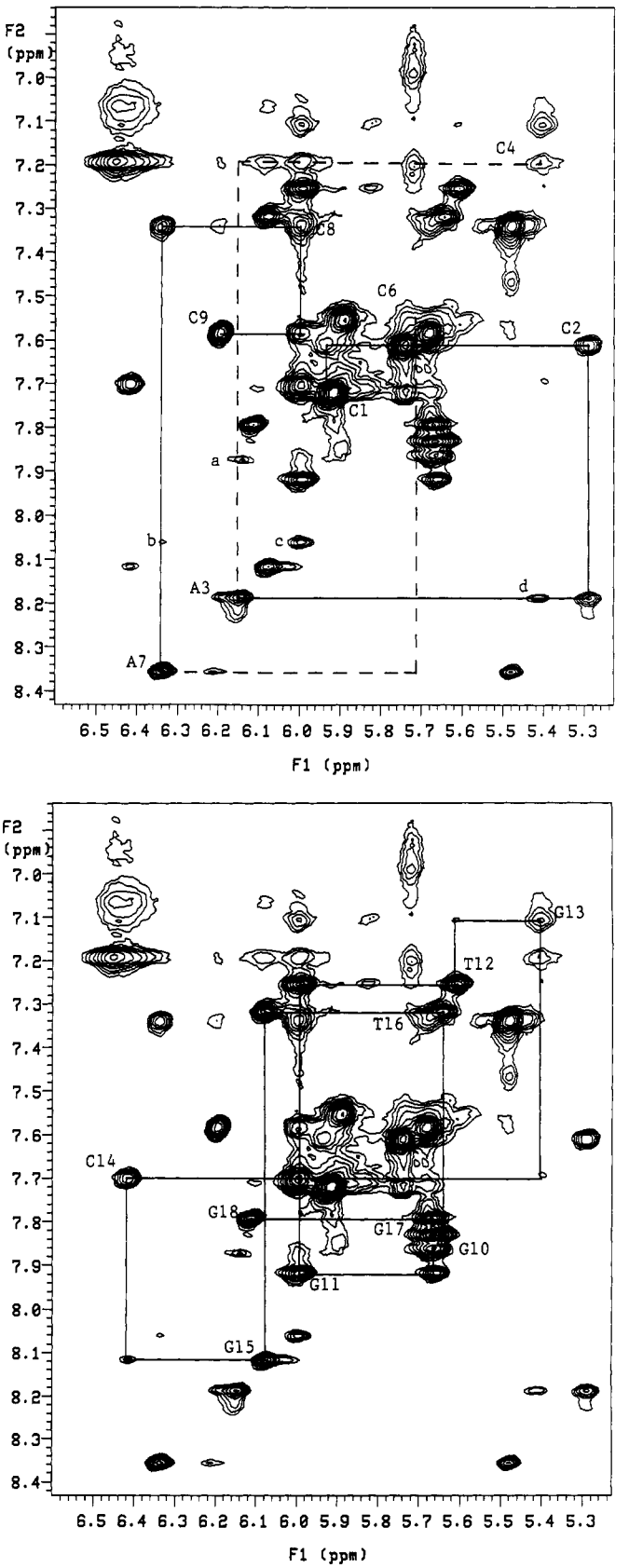

FIGURE 4: Base to H1′ region of the NOESY spectrum recorded in D_2O at 32 °C with a mixing time of 450 ms used for the assignment of the base and H1′ protons with connectivities traced out for (A, top) the modified strand and (B, bottom) the unmodified strand. The intranucleotide base to H1′ NOE cross peaks are labeled as C1, C2, A3, etc. NOEs referenced in the text are labeled with lowercase letters. Solid lines trace out the connectivities between the observed NOE cross peaks while dashed lines trace out the connectivities to the locations of anticipated but unobserved NOE cross peaks.

Table II: Chemical Shifts of the Nonexchangeable Protons in d(CCAC[AAF-G]CACC)·d(GGTGCGTGG)[a]

base	H8/H6	H2	H1′	H2′	H2″	H3′	H4′	H5	CH_3
C^1	7.76		5.98	2.04	2.49	4.68	4.14	5.96	
C^2	7.62		5.32	2.18	2.38	4.86	4.13	5.76	
A^3	8.20	7.89	6.16	2.58	2.58	5.19	4.40		
C^4	7.20		5.39/5.43[b]	0.30[c]	1.47[c]	4.44	3.80	6.44	
G^5			5.74/5.50[b]	[2.24/3.60/3.15][d]					
C^6	7.57		5.74	2.24	2.24	4.79		5.91	
A^7	8.37	8.08	6.34	2.93	2.93	5.08	4.42		
C^8	7.38		6.04	2.09	2.44	4.81	4.19	5.52	
C^9	7.66		6.24	2.29	2.29	4.54	4.04	5.80	
G^{10}	7.88		5.67	2.51	2.64	4.83	4.21		
G^{11}	7.95		6.02	2.73	2.73	5.00	4.40		
T^{12}	7.27		5.64	1.78	1.78	4.69	4.15		1.52
G^{13}	7.16		5.43	1.95	1.47	4.69	4.20		
C^{14}	7.71		6.41	2.33	2.47	4.99	4.05	5.97	
G^{15}	8.13		6.08	2.76	2.78	4.99	4.45		
T^{16}	7.32		5.66	2.04	2.26	4.86	4.19		1.53
G^{17}	7.84		5.68	2.66	2.71	4.98	4.35		
G^{18}	7.82		6.14	2.53	2.37	4.66	4.21		

[a] The data were recorded at 32 °C for a 4.6 mM sample; values given are in parts per million referenced to the water resonance at 4.72 ppm. [b] Found in two locations in slow exchange (see text). [c] Assignments are tentative and could be reversed. [d] The individual resonances have not been assigned (see text).

protons, however, do not exhibit observable NOEs to C4-H5. These cross peaks may be too broad to detect because the C4-H5 resonance is broadened, presumably due to chemical exchange.

The one remaining imino proton resonance (at 11.88 ppm) is assigned to the AAF-G5 imino proton. An NOE is observed between the AAF-G5 imino proton and the AAF-G5 amino protons (cross peak G in Figures 3A and 3C). The AAF-G5 amino protons are the only guanine amino proton resonances observed in the NOESY spectrum in Figure 3. Guanine amino proton resonances are not usually observed for Watson–Crick base pairs, and thus observation of the AAF-G5 amino proton resonance is consistent with a syn conformation for AAF-G5. The syn orientation of AAF-G5 precludes Watson–Crick hydrogen bonding to C14; in fact, we find no evidence of hydrogen bonding between the AAF-G5 and C14 bases. In neither one-dimensional nor two-dimensional NMR experiments were we able to observe an NOE between the G5 imino proton and adjacent C4·G15 or C6·G13 imino protons, which also is consistent with the AAF-G5 base having a syn conformation.

The syn conformation of the AAF-G5 moiety precludes the use of guanine imino to cytosine amino proton NOEs for locating the C14 amino protons. We do not observe NOEs between C14-H5 and any amino protons. Because all amino to amino cross peaks in Figure 3B have been assigned, we are unable to locate the C14 amino proton resonances.

Unanticipated NOEs are observed from the G5 imino proton to the A3-H3′ proton (cross peak U in Figure 3C) and from the G5 imino proton to the (overlapped) A3-H2′ and A3-H2″ protons (cross peak V in Figure 3C). These NOEs characterize the structure of the AAF-9-mer in that they place restraints on the location of the AAF-G5 imino proton, as discussed below.

One-dimensional spectra recorded in H_2O as a function of temperature show that the imino proton resonances of the AAF-9-mer broaden as two groups (Figure B, Supplementary Material). The C2·G17, A3·T16, and C4·G15 imino proton resonances broaden as one group, and the C6·G13, A7·T12, and C8·G11 imino protons resonances broaden as an independent group. The C2·G17, A3·T16, and C4·G15 imino proton resonances are observed at higher temperatures than the AAF-G5, C6·G13, A7·T12, and C8·G11 imino proton resonances. From this we conclude that the presence of the AAF moiety on the AAF-G5 base destabilizes the duplex in the 3′ direction of the modified strand more than the 5′ direction. We show below that the fluorene moiety is stacked on G15, which may be an important factor in the differential stability of the two ends of the AAF-9-mer duplex, as the stacking of the fluorene ring may help stabilize the duplex in the 5′ direction of the modified strand.

Assignment of the Nonexchangeable Protons. Several of the DNA base and sugar H1′ proton resonances (Figure 2) are broader than expected for this size oligomer. This broadening is a result of chemical exchange which complicates resonance assignments as well as analysis of NOESY data for distance restraints. In the unmodified 9-mer (O'Handley and Krugh, unpublished data) the assignment of the base and sugar proton resonances followed from a straightforward analysis of NOESY and TOCSY spectra using standard strategies (Pardi et al., 1983; Nerdal et al., 1988; van de Ven & Hilbers, 1988), and thus there appears to be nothing unusual about the 9-mer sequence selected for the present study. For the AAF-9-mer duplex, assignments for base and sugar protons of the three base pairs at either end of the duplex were completed from initial NOESY and COSY spectra recorded at the Syracuse University NIH NMR facility in 1985 (Sanford, 1986). However, for the AAF-9-mer duplex the assignment of the resonances for the central three base pairs was complicated by overlap of resonances, missing cross peaks, unusual chemical shifts, complications introduced by the presence of chemical exchange cross peaks, and loss of the H8 proton in the AAF-G5 base (Figure 1). Most of the nonexchangeable protons were assigned from spectra recorded at 32 °C, where resonances were reasonably well resolved. However, it was necessary to record NOESY and TOCSY spectra at 5, 12, 20, 25, and 32 °C to complete the assignments given in Table II. For brevity, only an overview of the assignment methodology is presented below; the details of the complete assignment strategies are presented separately (O'Handley, 1991).

Base and H1′ Proton Assignments for the AAF-9-mer Duplex. The cytosine base proton resonances were identified by their H5 to H6 cross peaks and the thymine base proton resonances by their methyl to H6 cross peaks in both NOESY and TOCSY spectra (Figure C, Supplementary Material). As shown in Figure 4B, all base to H1′ NOE connectivities were observed for the unmodified strand (G10–G18).

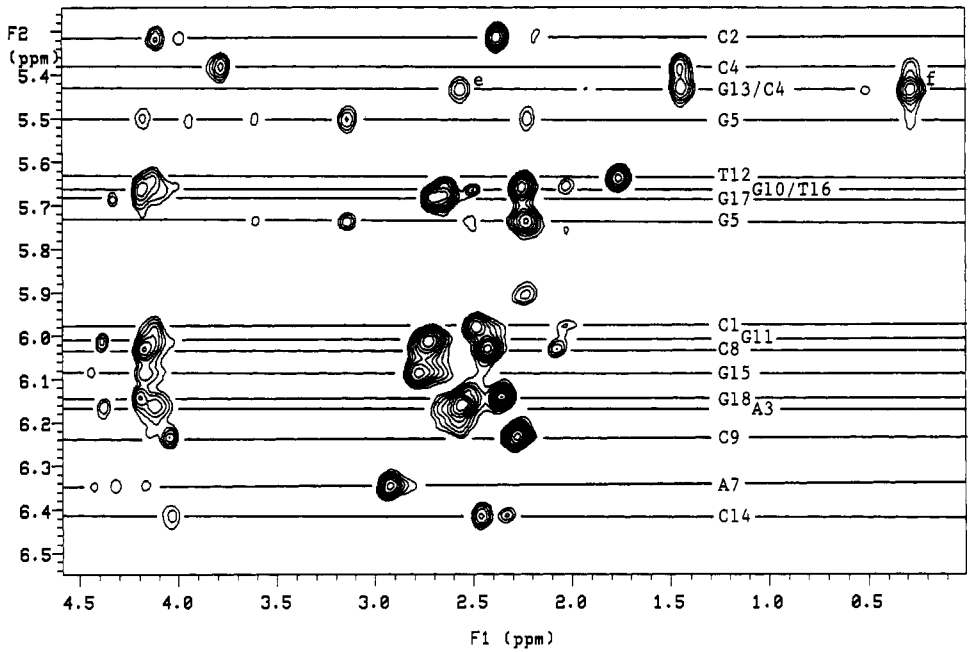

FIGURE 5: H1′ to H2′/H2″ and H4′ region of the NOESY spectrum recorded in D_2O at 32 °C with a mixing time of 100 ms used for assigning the H2′, H2″, and H4′ protons and for determining NMR distance restraints.

In the AAF-modified strand (C1–C9) the base to H1′ NOE connectivities could be traced from C1-H6 to A3-H1′ (Figure 4A). The base to H1′ connectivities are not observed for any of the central three nucleotides but resume with the A7-H8 to A7-H1′ cross peak and continue to the end of the strand (C9-H1′). Base and H1′ proton resonances which could not be assigned from the base to H1′ connectivities due to missing cross peaks or overlapping resonances were assigned via alternate connectivity pathways.

Assignment of the C4-H6 resonance at 7.20 ppm was made from the H5-H6 cross peak in the DQCOSY and TOCSY spectra (Figure C, Supplementary Material). The C4-H1′ resonance was assigned from an unexpected cross peak to A3-H8 (cross peak d in Figure 4A), which may arise from spin diffusion in a minor conformer. The C4-H1′ resonance is in slow exchange between 5.39 and 5.43 ppm, with the predominant conformation represented by the 5.39 ppm resonance (deduced from a TOCSY spectrum, as discussed below).

C6-H6 was assigned from the base to H3′ connectivities and the base to H2′/H2″ connectivities (Figures D and E, Supplementary Material). The C6-H6 to C6-H5 cross peak confirmed this assignment. At 20 °C (data not shown), the C6-H6 to C6-H1′ NOE was resolved from an overlapping cross peak at 32 °C, allowing assignment of the C6-H1′ resonance. The internucleotide NOE between C6-H1′ and A7-H8 was not observed, even at long mixing times.

Base proton assignments were confirmed in the base to H2′/H2″ and base to H3′ regions of the NOESY spectrum (Figures D and E, Supplementary Material). These regions of the NOESY spectrum were also used for initial assignment of the H2′, H2″, and H3′ protons. All of the H8/H6 to H2′/H2″ and H8/H6 to H3′ NOE connectivities were observed at long mixing times for the G10 to G18 nucleotides. As in the base to H1′ region, many of the base to H2′/H2″ and base to H3′ NOEs were missing in the AAF-modified strand (C1 to C9). Base to H2′/H2″/H3′ NOEs could be traced from C1 to A3, but there was no indication of NOEs between any A3 sugar protons and C4-H6. The usual base to H2′/H2″/H3′ NOE connectivities resumed at C6 and continued to C9. Sugar protons which could not be assigned from base to sugar NOEs were assigned from DQCOSY and TOCSY spectra.

Assignment of H2′ and H2″ Protons. The H2′ and H2″ protons may be distinguished from one another by their coupling pattern with H1′ in a DQCOSY spectrum (Figure F, Supplementary Material). Generally, the H1′-H2′ cross peak is characterized by a strong active coupling and a weak passive coupling, while the H1′-H2″ cross peak is generally characterized by a more complex coupling pattern (Zhou et al., 1988). Nonoverlapping H2′ and H2″ resonances could be distinguished in this way, except for the C4, AAF-G5, and G13 resonances. The H1′-H2′ and H1′-H2″ coupling patterns are a function of the sugar pucker, and thus assignment of H2′ and H2″ from DQCOSY coupling patterns must be made with caution (Schmitz et al., 1990). However, the H1′ proton is closer to the H2″ proton than to the H2′ proton for all sugar conformations, and thus the relative intensities of the H1′ to H2′ and H1′ to H2″ cross peaks in the 100-ms mixing time NOESY spectrum (Figure 5) were compared to verify the H2′ and H2″ assignments. All of the H2′ and H2″ assignments were confirmed in this way, except for the C4, AAF-G5, and G13 resonances, whose assignments are discussed below.

Sugar Proton Assignments from TOCSY Spectra. In the TOCSY spectrum recorded at 32 °C with a mixing time of 100 ms, all scalar connectivities from H1′ to H2′, H2″, and H3′ were observed, as were many of the H1′ to H4′ scalar connectivities (Figure 6). Many of the H4′ protons which could not be assigned through a scalar connectivity to H1′ could be assigned through a scalar connectivity to H2′ and H2″. Also, nearly all of the intranucleotide H1′ to H4′ NOEs were observed in the 100-ms mixing time NOESY at 32 °C (Figure 5). The difficult assignments, those of C4, G5, C6, and G13, are discussed below.

Assignment of C4 Sugar Protons. The assignment of the C4 sugar protons is complicated by both chemical exchange and weak NOEs between the C4-H6 proton and the C4-H2′ and C4-H2″ protons. The C4-H1′ proton resonance is found at both 5.39 and 5.43 ppm (e.g., Figure 5). Tentative assignments for C4-H2′ and C4-H2″ were obtained from the H1′ to H2′/H2″ region of the NOESY, TOCSY, and

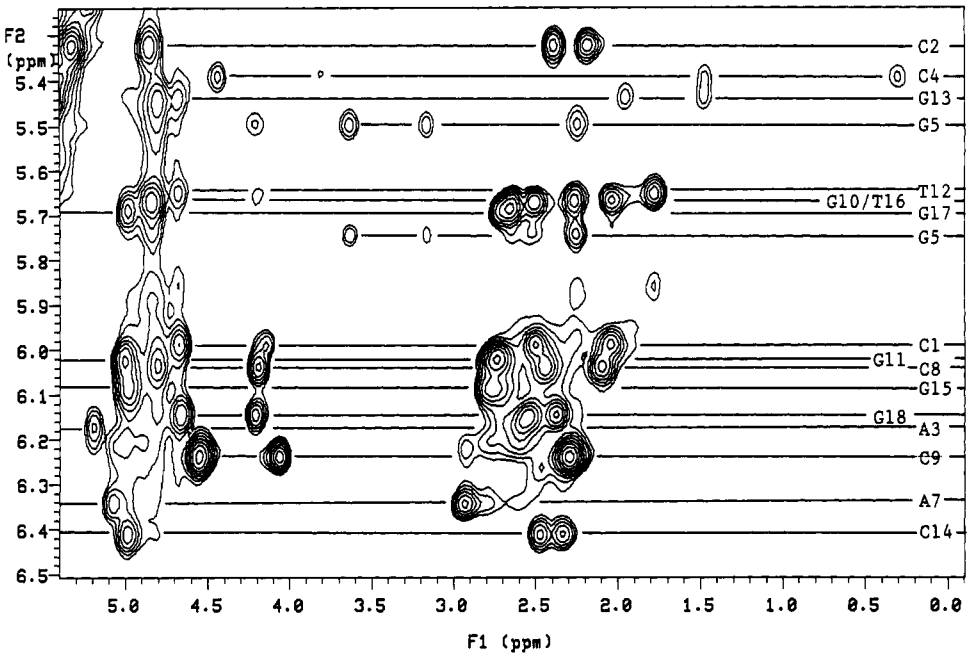

FIGURE 6: H1′ to H2′/H2″, H3′, and H4′ region of the TOCSY spectrum recorded in D_2O at 32 °C with a mixing time of 100 ms used for the assignment of sugar protons. The locations of the H1′ resonances are indicated.

DQCOSY spectra. In the DQCOSY spectrum the cross peak from the C4-H1′ proton resonance at 5.39 ppm to the H2′/H2″ proton resonance at 1.47 ppm is too weak to determine the coupling pattern, but the cross peak from 5.39 to 0.3 ppm is observable and exhibits a coupling pattern expected for an H1′ to H2′ cross peak. From this coupling pattern the resonance at 0.3 ppm has been tentatively assigned to C4-H2′ and the resonance at 1.47 ppm has been tentatively assigned to C4-H2″. TOCSY cross peaks (Figure 6) are observed between the C4-H1′ proton resonance at 5.39 ppm and the C4-H3′ (4.44 ppm), C4-H2′ (0.3 ppm), C4-H2″ (1.47 ppm), and C4-H4′ (3.80 ppm) proton resonances. However, in the 5.43 ppm slice, the only TOCSY cross peaks observed in Figure 6 are assigned to the overlapping G13-H1′ resonance, and thus we conclude that the chemical shift of the C4-H1′ proton in the predominant conformation is located at 5.39 ppm. A strong NOESY cross peak is observed from 5.43 to 0.3 ppm (cross peak f in Figure 5) which is assigned to an NOE between the C4-H1′ proton and the C4-H2′/H2″ proton. There is no equivalent TOCSY cross peak at this location in Figure 6, which is consistent with having a short internuclear distance between these protons in a minor conformation. An unusual conformation of the minor conformer is also illustrated by a NOESY cross peak between a resonance at 5.43 ppm and a resonance at 2.58 ppm (cross peak e in Figure 5); we assign this cross peak to a C4-H1′ to A3-H2′/ A3-H2″ NOE; although other assignments might be possible, this unusual NOE is consistent with the NOESY cross peak between the A3-H8 proton and the C4-H1′ proton (cross peak d in Figure 4A in the 450-ms mixing time NOESY spectrum). A C4-H1′ to A3-H2′/ A3-H2″ cross peak is not observed in the 5.39 ppm slice of the C4-H1′ resonance, nor is there a TOCSY cross peak observed in the 5.43 ppm slice at 2.58 ppm. The resonance for C4-H2′, located at 0.3 ppm, is in an unusual upfield location for an H2′ (or H2″) resonance. The C4-H3′ (4.44 ppm) and C4-H4′ (3.80 ppm) resonances are also upfield of the other H3′ and H4′ resonances.

Assignment of AAF-G5 Sugar Protons. The absence of an H8 proton on the AAF-G5 base eliminates the possibility of intranucleotide base to sugar NOEs for AAF-G5. Also, no internucleotide NOEs were observed from the AAF-G5 sugar protons to C6-H6. The AAF-G5 sugar protons were assigned from scalar coupling and NOEs among one another. The resonances at 5.55 and 5.70 ppm were both determined to be AAF-G5-H1′ resonances and the resonances at 2.24, 3.15, and 3.60 ppm were determined to be AAF-G5-H2′ and AAF-G5-H2″ resonances from the DQCOSY experiment. The H2′/H2″ resonances at 3.15 and 3.60 ppm are downfield of the other H2′/H2″ resonances. Due to chemical exchange, the individual assignments of the AAF-G5-H2′/H2″ protons were not determined. AAF-G5-H3′ and AAF-G5-H4′ resonances could not be located. Because one of the AAF-G5-H1′ resonances overlaps the C6- H1′ resonance and one of the AAF-G5-H2′ or H2″ resonances overlaps the C6-H2′/H2″ resonance at 32 °C, it is difficult to distinguish AAF-G5 resonances from C6 resonances at this temperature. The overlap between the AAF-G5-H2′ or H2″ resonance and the C6-H2′/H2″ resonance is eliminated at other temperatures, and the cross peaks belonging to AAF-G5 could be differentiated from those belonging to C6.

Assignment of C6 Sugar Protons. C6-H2′, C6-H2″, and C6-H3′ were assigned from NOE connectivities in the base to sugar regions of the NOESY spectrum. As noted above, C6-H1′ was assigned from an NOE to C6-H6. No cross peaks were observed between C6-H1′ and other sugar protons in NOESY, TOCSY, or DQCOSY spectra, but cross peaks were observed from C6-H2′ to C6-H3′ and from C6-H2″ to C6-H3′ in NOESY and TOCSY spectra.

Assignment of G13 Sugar Protons. For G13, the H1′ to H2′ and the H1′ to H2″ cross peaks are weak in the DQCOSY spectrum. The cross peak from 5.43 to 1.95 ppm is observable with a coupling pattern similar to the other H1′ to H2′ cross peaks, but the expected cross peak from 5.43 to 1.47 ppm is apparently too weak to be observed. The assignment of 1.95 ppm as the G13-H2′ resonance and 1.47 ppm as the G13-H2″ resonance is supported by the relative NOE intensities in the 100-ms mixing time NOESY spectrum. The strong NOE from 5.43 to 1.47 ppm is assigned as the G13-H1′ to G13-H2″ NOE. The weak NOE from 5.43 to 1.95 ppm is as expected for G13-H1′ to G13-H2′. The strong NOE to G13-H8 in the H2′/H2″ region at 1.95 ppm (with an intensity comparable to that of a C-H5 to C-H6 NOE) is assigned as

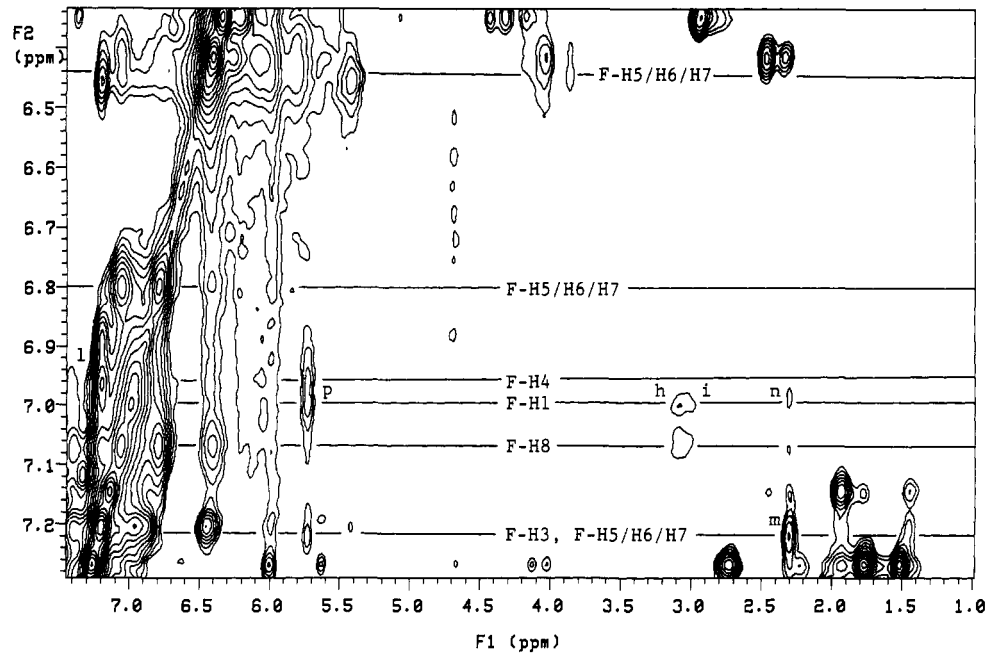

FIGURE 7: Portion of the NOESY spectrum recorded in D_2O at 32 °C with a mixing time of 450 ms used for the assignment of the AAF protons. NOEs are observable between carcinogen protons and from carcinogen protons to DNA protons. Labeled cross peaks are referenced in the text.

Table III: Chemical Shifts of the Acetylaminofluorene Protons in d(CCAC[AAF-G]CACC)·d(GGTGCGTGG)[a]

proton	chemical shift	proton	chemical shift
F-H1	7.00	F-H8	7.07
F-H3	7.22	F-H9/F-H9′[b]	3.05/3.10
F-H4	6.94	F-CH_3	2.30
F-H5/F-H6/F-H7[b]	6.45/6.80/7.20		

[a] The data were recorded at 32 °C for a 4.6 mM sample; values given are in parts per million referenced to the water resonance at 4.72 ppm. [b] The individual resonances have not been assigned.

the G13-H8 to G13-H2′ NOE. Cross peaks in the TOCSY spectrum corresponding to scalar coupling from G13-H1′ to G13-H2′, G13-H2″, and G13-H3′ are consistent with these assignments.

Assignment of the 2-Acetylaminofluorene Protons. The chemical shift of the acetyl methyl protons (F-CH_3) is 2.30 ppm, while the F-H9/H9′ protons have chemical shifts of 3.05 and 3.10 ppm. The broad resonances in the 6.5–7.15 ppm region of the spectra in Figure 2 are from the aromatic protons of the 2-acetylaminofluorene moiety. The F-H5, F-H6, F-H7, and F-H8 protons were differentiated from the F-H1, F-H3, and F-H4 protons by the coupling patterns observed in TOCSY spectra and from cross peaks observed in NOESY spectra. The F-H8 proton was assigned from NOEs to the F-H9 and F-H9′ protons. The F-H5, F-H6, and F-H7 protons, however, could not be assigned individually. The F-H1 proton was also assigned from NOEs to the F-H9 and F-H9′ protons (cross peaks h and i in Figure 7). The F-H3 proton was assigned by observation of NOEs to both F-H1 and the F-CH_3 protons (cross peaks l and m in Figure 7). The chemical shifts of the 2-acetylaminofluorene protons are summarized in Table III.

Chemical Exchange. Several resonances from protons located in the central portion of the duplex exhibit chemical exchange cross peaks. For example, in the base and H1′ regions of NOESY and TOCSY spectra, the C4-H1′, G5-H1′, A7-H2, T12-H1′, and G13-H8 protons exhibit chemical exchange cross peaks near the diagonal. Each proton, however, exhibits one major resonance which we estimate represents ≥70% of the total intensity in one-dimensional spectra, and, therefore, we conclude that one conformation of the adduct predominates. The presence of more than one conformation of the AAF-9-mer duplex was a motivating factor in performing the molecular dynamics simulation without the use of distance restraints.

Magnesium chloride was added to determine if magnesium ions might stabilize one structure of the AAF-9-mer duplex and thus eliminate the complicating effects of chemical exchange. However, the addition of up to 15 mM Mg^{2+} (five magnesium ions per duplex) did not alter the line widths in one-dimensional spectra. None of the DNA proton resonances known to participate in chemical exchange (e.g., G13-H8, C4-H1′, C4-H2″, and the carcinogen proton resonances) narrowed as the magnesium chloride concentration was increased, which we interpret as evidence that chemical exchange was not eliminated.

Overall Structural Features. For the outer three base pairs on either end of the duplex, the relative volumes of base to sugar NOESY cross peaks, as well as the relative volumes of sugar to sugar cross peaks in the 100-ms mixing time NOESY spectrum (Figure 6 and data not shown), are consistent with a right-handed B-type DNA conformation. From this we conclude that the most prominent changes from a B-form type structure are localized to the central region of the modified duplex.

NOEs observed at 6 °C in H_2O between the AAF-G5 imino proton and A3-H2′/H2″ and A3-H3′ (cross peaks U and V in Figure 3C) indicate that AAF-G5 is in a syn conformation. The C4 base to C4 sugar NOEs are weak, and thus the C4 glycosidic bond torsion angle cannot be obtained from these data. All other bases are in the anti orientation about their glycosidic bond, as evidenced by strong intranucleotide base to H2′ NOEs, and weak base to H1′ NOEs.

All base pairs, except for AAF-G5 and C14, are Watson–Crick hydrogen bonded as evidenced by guanine imino proton to cytosine amino proton NOEs or by thymine imino proton to adenine H2 NOEs (Figure 3A). Since AAF-G5 is in the

syn orientation, Watson–Crick base pairing between AAF-G5 and C14 is precluded; in fact, no evidence was obtained for any hydrogen bonding between the AAF-G5 and C14 bases.

The NOEs observed from F-H1 and F-H3 to AAF-G5-H1′ or C6-H1′ (the AAF-G5-H1′ and C6-H1′ resonances overlap) at a mixing time of 100 ms (cross peaks o and p in Figures 6 and 7B) locate these fluorene protons in the minor groove, again showing that AAF-G5 adopts a syn orientation about the glycosidic bond. The NOE from AAF-G5-H1′ or C6-H1′ is stronger to F-H1 than to F-H3 (cross peaks p and o in Figure 7B), while the NOE from the methyl protons of the carcinogen is stronger to F-H3 than to F-H1 (cross peaks m and n in Figures 6 and 7B). These relative intensities help to determine the orientation of the carcinogen moiety. Weak NOEs are observed at long mixing times from the F-H1 proton to C4-H1′, C4-H2′, and C4-H2″. At 6 °C in H_2O solution an NOE is observed between the C4-G15 imino proton and the F-H3/F-H5/F-H6/F-H7 resonance (peak W in Figure 3A). These NOEs indicate stacking of the fluorene ring on the C4·G15 base pair on the 5′ side of the modified guanine, as will be seen in the structure of the AAF-9-mer presented below.

NMR Distance Restraints. The volumes of the cross peaks from a NOESY spectrum recorded at 32 °C with a mixing time of 100 ms were measured and used to determine distance restraints. NMR-derived distances were calculated by taking the sixth root of the ratio of the C-H5 to C-H6 cross peak volume to the volume of the cross peak in question (Gronenborn & Clore, 1985; van de Ven & Hilbers, 1988). These calculations provide numerical distances from which the upper and lower bounds were derived by including estimates of error. For example, the presence of a strong NOE between the F-H1 proton and the AAF-G5-H1′ proton led to the use of an upper bound of ≤3.2 Å. The weak NOE observed between the F-H1 protons and the C4-H2′ protons led to the use of an upper bound of ≤5.0 Å. Lower bounds were used for some base to sugar protons in those cases where the observed NOE cross peak was much weaker than the value expected for B-form DNA. A list of the NMR distance restraints used in energy minimization is found in Table IV. The presence of chemical exchange in the spectra raises the possibility that the derived distance restraints may contain contributions from more than one conformation, and thus some distances may be weighted to the shorter values. This is a concern in any NMR-derived structure but is of particular importance here due to the presence of more than one conformer. As described below, we address this possibility in the energy minimization calculations by releasing the restraints in the last stages of minimization and by performing molecular dynamics calculations without NMR restraints.

Energy-Minimized Structures. The tetramer d(A3-C4-[AAF-G5]-C6)·d(G13-C14-G15-T16) was selected for the initial energy minimization studies because this included the region of the AAF-9-mer around the AAF moiety. Restraints 1–6 of Table IV were used at this stage of the minimization studies, as was the hydrogen-bonding penalty function at the A3·T16, C4·G15, and C6·G13 base pairs (consistent with NMR data). The hydrogen-bond penalty function was not used at AAF-G5 because the NMR data showed no evidence for hydrogen bonding between AAF-G5 and C14.

The orientation of the AAF moiety in relation to the guanine to which it is bound was then investigated with a series of energy minimization trials that employed distance restraints. In these trials the DNA starting conformation was a B-DNA fiber diffraction model (Arnott et al., 1976) with the AAF-G5 glycosidic torsion angle rotated to syn ($\chi = 60°$; see Figure 1 for torsion angle definitions). The AAF-G5 orientation space was searched, with distance restraints 1–6 of Table IV, in the following energy minimization trials: $\alpha' = 0°, 90°, 180°, 270°$, in combination with $\beta' = 0°, 90°, 180°, 270°$. γ' and δ' were started at 0° and 60°, respectively; the choice for γ' was dictated by earlier studies (Hingerty & Broyde, 1982a,b) which indicated the 0° domain to be preferred over 180°. These 16 starting conformations were employed with four combinations of restraints 2 and 3 of Table IV, for a total of 64 trials.

Table IV: Experimental Distance Restraints (Å) Used in Energy Minimization Calculations and Observed Distances in K9DE, the Energy-Minimized Structure, and during Unrestrained Molecular Dynamics Simulations

NOE no.[a]	atom pair	distance (Å) restraint used in energy min.[b]	distance (Å) in K9DE	"NOE averaged distance" during MD[c]
1	G5-H1 to A3-H3′	≤4.5	4.6	3.1
2[a]	AAF-H1 to G5-H1′	≤3.2	2.7	2.9
3[a]	A3-H2′ to C4-H1′	≤3.5	3.8	4.5[d]
4	G13-H3′ to C14-H6	≤3.5	3.6	3.0
5	C14-H4′ to G15-H8	≤4.0	4.2	5.7
6	A3-H2″ to C4-H6	≥3.5	4.7	4.0
7	G13-H8 to C14-H5	≤5.0	4.0	4.0
8	AAF-H1 to C4-H2′	≤5.0	3.2	2.7
9	G13-H8 to G13-H2′	≤2.5	3.6	3.3
10	A3-H8 to A3-H2′	≤2.5	3.7	3.7
11	T12-H2′ to G13-H8	≥2.6	3.7	2.5
12	T12-H2″ to G13-H8	≥2.6	2.3	2.6
13	G13-H2′ to C14-H6	≥2.6	2.4	2.6
14	G13-H2″ to C14-H6	≥2.8	3.7	3.3
15	C14-H1′ to G15-H8	≥2.8	2.7	4.2
16	A3-H2′ to C4-H6	≥3.5	3.2	2.5
17	C6-H2″ to A7-H8	≥2.6	2.1	3.2

[a] Due to overlap in the spectrum, distance restraints 2 and 3 were considered in pairs, and searches were made for four possible combinations, as explained in the text. [b] Volumes of the cross peaks were used to obtain estimates of internuclear separation which were then interpreted in terms of either maximum or minimum distance restraints for energy minimization calculations using DUPLEX. [c] The internuclear distances were sampled every picosecond and then averaged to take into account the r^{-6} dependence of the NOE ($r_{\text{NOE average}}$ = [average of r_{ij}^{-6}]$^{-1/6}$). [d] This distance restraint comes from cross peak "e" in Figure 5; the C4-H1′ proton is found at two locations, and thus this NOE cross peak may arise from an unusually close distance in a minor conformer.

The results were evaluated by employing eq 1 and 2 to calculate F_N and F_{NN} as indexes of goodness of fit to the NMR data, with d now the achieved distance in the energy minimum. At this point, a single trial of the 64 stood out with a better goodness of fit than any other, with values (in kcal/mol) of $F_N = 1.9$ and $F_{NN} = 0.0$, using W_N and $W_{NN} = 15$ kcal/(mol·Å^2). The energy of this structure was −160.8 kcal/mol, and it was second lowest in energy of the 64 trials. By contrast, the lowest energy structure (−169.6 kcal/mol) had goodness of fit indexes $F_N = 31.2$ and $F_{NN} = 1.4$, while the structure with the second best goodness of fit indexes had values of $F_N = 2.2$ and $F_{NN} = 0.1$, but the energy was much higher, at −132.4 kcal/mol. The structure with the best goodness of fit indexes revealed that constraints 2 and 3 of Table IV were the better fitting distances of each pair (from overlapped resonances). Constraints 7 and 8 were then added, and the tetramer that best fit the distance restraints from the previous stage was energy minimized again. The possibility that γ' might occupy the 180° rather than the 0° domain was explored by rotating this torsion angle to 180° and minimizing again with restraints, but this domain proved to be somewhat higher in energy.

In the next stages, the tetramer was built, stepwise, to the duplex AAF-9-mer, by first adding the minimized B-form

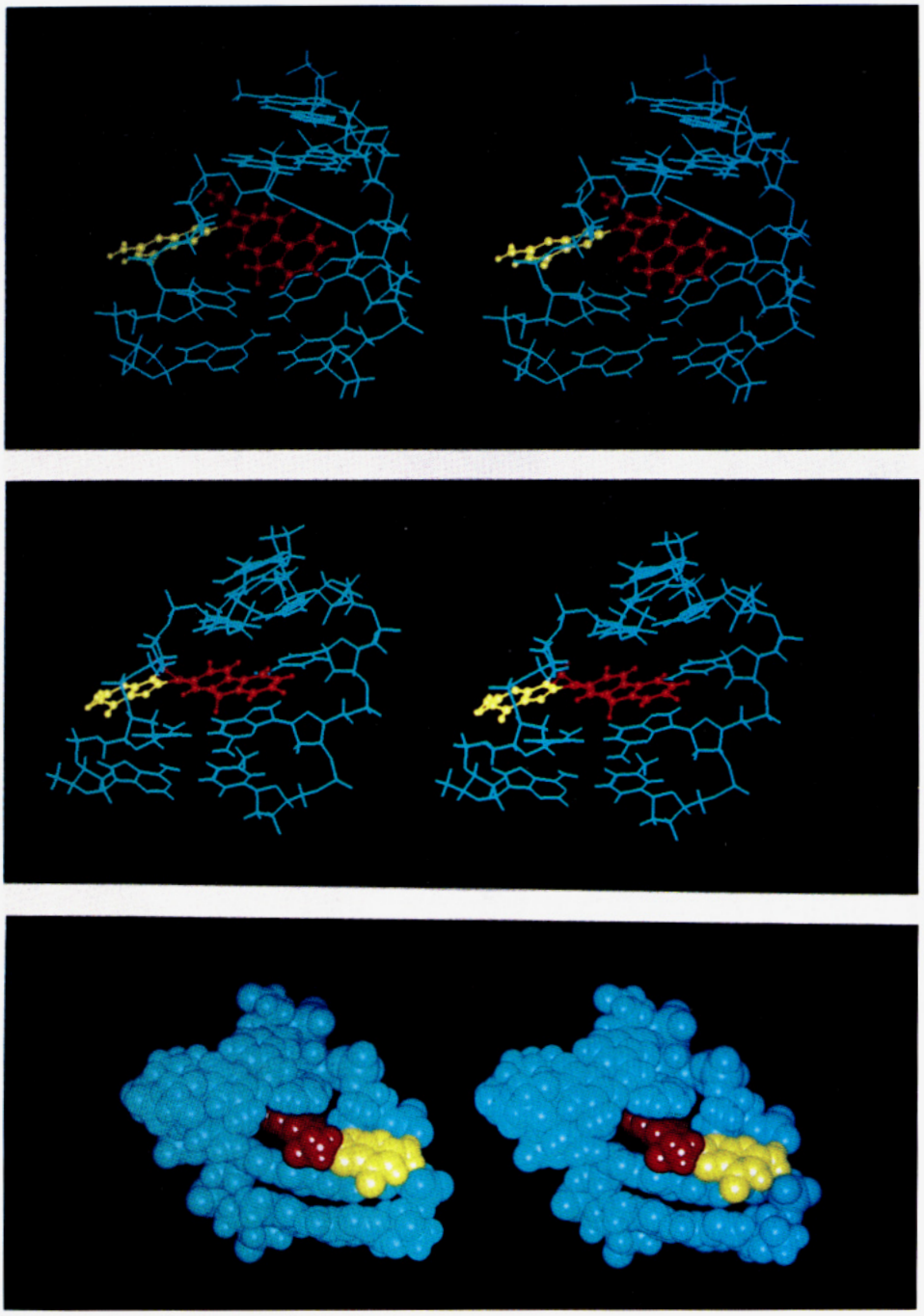

FIGURE 8: Stereoviews of the central 5-base-pair region of the AAF-9-mer, d(A3-C4-[AAF-G5]-C6)·d(G13-C14-G15-T16): (top) K9DE, the energy-minimized structure; (center) K9DE160, the structure obtained after 160 ps of unrestrained molecular dynamics; (bottom) space-filling model of K9DE160 as viewed from the major groove. The fluorene moiety is shown in red, the AAF-G5 base is yellow, and the remaining atoms are blue. Torsion angles χ, α', β', γ', and δ' at AAF-G5 (see Figure 1) are 62, 44, 23, 37, 23 and 37, 31, 18, 40, 13 for K9DE and K9DE160, respectively. Coordinates of these two structures and the structure in Figure 11 are available from the authors.

duplex block of residues 1 and 2, minimizing the 6-mer, and then adding a residue at a time, followed by minimization, with distance restraints retained at each stage. Once the 9-mer was built, additional restraints 9–17 were added and another round of minimization was undertaken. Subsequently, the hydrogen-bond penalty function and then the distance restraints were released with energy minimization at each step, yielding finally an unrestrained structure, K9DE. In general, there is agreement between the distances estimated from NOESY cross peaks and the distances in the unrestrained energy-minimized structure, and thus we believe the structure shown as K9DE is characteristic of the major conformation of the AAF-9-mer. Before release of the NMR constraints, essentially all the observed distances were within the limits derived from the analysis of the 100-ms mixing time NOESY data or close to these values. The release of the constraints resulted in the increase in the length of restraint 10, along with smaller changes in other values. Although the overall conformation (Figure 8) remained unchanged as the restraints were released, it is possible that one (or more) of the restraints may be due to a minor conformation of the AAF-9-mer. Restraint 3, which is derived from cross peak e in Figure 5, is a possible candidate because the C4-H1′ proton exhibits chemical exchange. Fortunately, the important conformational features of the AAF-9-mer are not influenced by this complication.

Molecular Dynamics Calculations. The energy-minimized K9DE structure was used as the starting structure in molecular

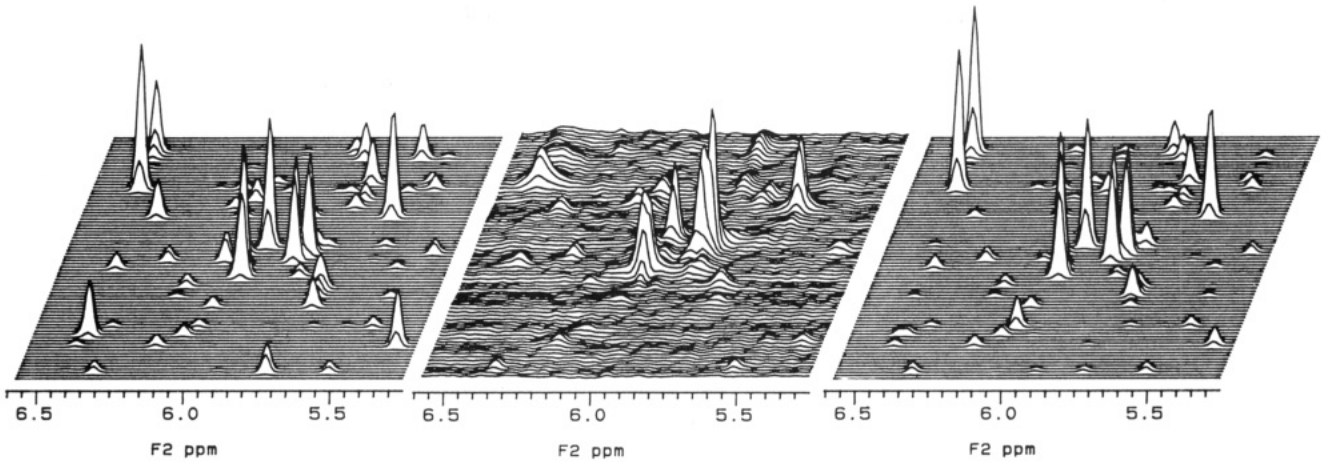

FIGURE 9: Calculated and experimental NOESY spectra for the base to H1′ region: (left) spectrum calculated for K9DE, the structure obtained from molecular mechanics calculations; (center) experimental spectrum for a 100-ms mixing time experiment; (right) calculated average spectrum for the structures every 5 ps from 90 to 210 ps in the molecular dynamics simulations.

dynamics simulations using the program AMBER 3.1 (Singh et al., 1988). Solvent and sodium ions were included to simulate the solution environment. Because the starting structure was the energy-minimized structure derived with use of NMR restraints during all but the last stages of minimization, the molecular dynamics simulations were carried out without use of restraints. The absence of distance restraints is intended to enhance the sampling of conformational space and to reduce the chance of bias in the structure that might arise if one (or more) of the restraints used in the energy minimization calculations was due to a short distance present in a minor conformer that is a longer distance in the predominant conformer. A plot of the root-mean-square deviation of the AAF-9-mer from the starting structure is shown as a function of time in Figure G in the Supplementary Material, and a plot of the total energy of the system as a function of time is given as Figure H in the Supplementary Material.

The structure of K9DE after 160 ps of unrestrained molecular dynamics simulations was selected as a representative structure from the dynamics simulation and is shown as K9DE160 in Figure 8. The AAF-9-mer (Figure 8) exhibits both a dislocation and a bend in the helix axis at the modification site. A 200-ps simulation of unmodified B-DNA of the same sequence was run as a control and did not exhibit these characteristics. The presence of a bend in the helix is consistent with previous electrophoretic mobility experiments and chemical probe experiments on AAF-modified oligomers (Schwartz et al., 1989; Leng, 1990). While the NOEs observed in DNA provide good definition of local structure, the lack of long-range NOEs limits the ability to define curvature of a duplex (Powers et al., 1989; Nikonowicz et al., 1991), and thus we focus on the local structure at the site of AAF binding as shown in Figure 8.

To compare the internuclear distances during the simulation with the NMR derived restraints, an "NOE average distance" ($r_{\text{NOE average}}$ = [average of r_{ij}^{-6}]$^{-1/6}$) was computed for the 60–210-ps portion of the dynamics simulation. The initial portion of the dynamics trajectory was not used to allow for an equilibration period. As shown in Table IV, the AAF-G5-imino proton to A3-H3′ proton "NOE average" internuclear distance is 3.1 Å, a value consistent with the relatively strong NOE observed (cross peak U in Figure 3C) and in better agreement with the experimental data than the 4.6 Å found in K9DE. A plot of this distance during the simulation is given in Figure I in the Supplementary Material.

While most internuclear separations stayed within the selected experimental bounds or even improved slightly, a few strayed beyond them. The C14 base is not base paired, and the A3, C4, and G13 nucleotides exhibit chemical exchange, and thus it is plausible that a minor conformer contributes to the NOESY cross peaks. However, the location of the G5 base in the major groove and the stacking of the fluorene ring on the C4·G15 base pair with protrusion into the minor groove is well-defined in the major conformer.

Calculation of NOESY Spectra. The base to H1′ region of the NOESY spectrum provides important structural information on the conformation of a duplex. This region of the NOESY spectrum was calculated using the NMR2/Model software (NMRi Inc.) for K9DE, the structure obtained from energy minimization (Figure 9, left), and for the structures generated along the molecular dynamics simulation trajectory (Figure 9, right). Structures were selected every 5 ps from 90 to 210 ps during the unrestrained molecular dynamics simulation for the AAF-9-mer. We selected the 90–210-ps time domain as representative of the dynamics simulation, although the choice of where to begin the spectral simulation was somewhat arbitrary. Twenty-five structures (taken every 5 ps from 90 to 210 ps) were used to calculate the base to H1′ region of the NOESY spectra and were averaged to give the spectrum shown on the right of Figure 9. The base to H1′ region of the NOESY spectrum calculated from the molecular dynamics simulation (Figure 9, right) reproduces the experimental base to H1′ region of the spectrum within experimental error. We believe the agreement between the calculated spectrum and the experimental spectrum is another indication that the structures shown in Figures 8 and 10 are characteristic of the predominant conformation of the AAF-9-mer in solution.

Several base to H1′ cross peaks that were too large in the NOESY spectrum calculated from the energy-minimized structure (Figure 9, left) are in good agreement with the experimental spectrum in the NOESY spectrum calculated from the 25 structures selected every 5 ps in the 90–210-ps time domain (Figure 9, right). Two cross peaks in the upper-left corner of each calculated spectrum appear much larger than the corresponding peaks in the experimental spectrum although, in fact, the volumes of these cross peaks are in reasonable agreement with the experimental spectrum. The apparent discrepancy is due to chemical exchange broadening observed in the experimental spectrum. The NMR2/Model software assigned a single line width to all cross peaks, and

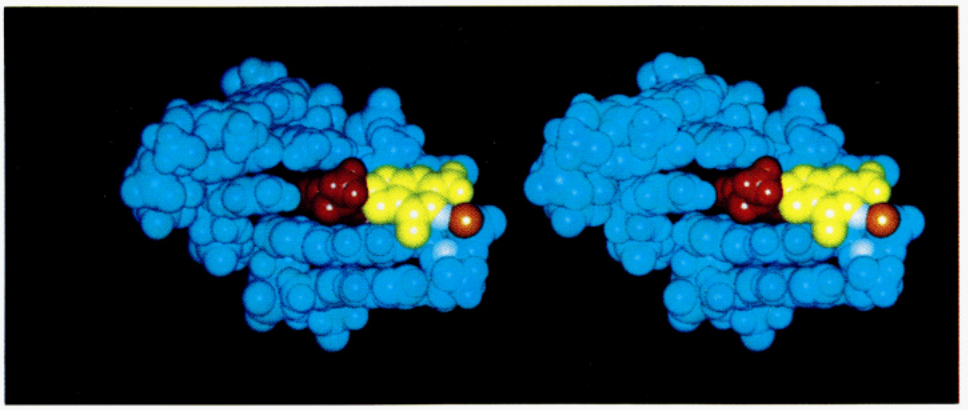

FIGURE 10: Structure of the d(-A3-C4-[AAF-G5]-C6-)·d(-G13-C14-G15-T16-) portion of the AAF-9-mer after 60 ps of unrestrained molecular dynamics simulation (K9DE60). The fluorene moiety is shown in red, the AAF-G5 base is yellow, the sugar–phosphate backbone and the remaining bases are blue, the AAF-G5-imino proton and the A3-H3′ protons are white, and the phosphate oxygen involved in transient hydrogen bond formation with the AAF-G5-imino proton is orange. Torsion angles χ, α', β', γ', and δ' at AAF-G5 (see Figure 1) for K9DE60 are 67, 50, 8, 44, and 33.

thus we were unable to simulate the different line widths observed in the experimental spectrum.

DISCUSSION

Structural Features. The three base pairs on each end of the AAF-9-mer duplex possess NOE patterns and intensities characteristic of right-handed B-DNA, and all bases are Watson–Crick hydrogen bonded except the complementary AAF-G5 and C-14 bases which show no evidence for hydrogen bond formation with each other. Even the C4·G15 base pair, which has an imino proton shifted upfield at 11.5 ppm, is Watson–Crick base paired. The AAF-G5 base is in a syn conformation, which is in accord with previous experimental studies (Grunberger et al., 1970; Fuchs & Daune, 1971, 1972; Evans et al., 1980; Singer & Grunberger, 1983). When the bulky N-acetyl group of AAF is attached to the C^8 position of guanine in the anti conformation, it is not easily accommodated near the sugar–phosphate backbone of the modified residue. Rotation of guanine to the syn conformation allows room for both the fluorene and acetyl moieties (Grunberger et al., 1970).

The NMR data show no evidence of hydrogen bonding between AAF-G5 and C14, its complementary base. Without hydrogen bonding the C14 base might be free to move and perhaps could be extrahelical. However, we observe G13-sugar ↔ C14-H6 ↔ C14-sugar ↔ G15-H8 NOE cross peaks as well as a G13-H8 to C14-H5 NOE cross peak. Thus the NOE data indicate that the C14 base is stacked within the helix. In the molecular dynamics simulations, the C14 base is located within the duplex as shown, for example, in Figure 8.

The AAF moiety (Figure 8) is stacked on the guanine of the adjacent C4·G15 base pair. The AAF-G5 base is displaced from the duplex, as in the base-displacement and insertion-denaturation models proposed many years ago (Grunberger et al., 1970; Fuchs & Daune, 1971, 1972). The modified guanine is positioned such that the distance between the AAF-G5-imino proton and A3-H3′ is 3.5 Å after 160 ps of molecular dynamics, a distance consistent with the cross peak observed between these protons (cross peak U in Figure 3C). The molecular dynamics simulations were done without NMR restraints, and thus the change in the location of the modified guanine during the simulation is due entirely to the AMBER forcefield. Although it is difficult to quantitate NOESY cross peaks in H_2O solution, we believe the magnitude of the AAF-G5-imino proton to A3-H3′ cross peak in Figure 3C is indicative of an internuclear separation in the 2.0–4.0 Å range. It is reassuring that the molecular dynamic simulations (without use of NMR restraints) resulted in an AAF-G5-imino proton to A3-H3′ proton internuclear distance within this range. It is also worth noting that a comparison of the base to H1′ region of the calculated and experimental NOESY spectra is essentially equivalent to monitoring 31 additional internuclear distances. The agreement of these spectra provides support for the important conformational features of the structure of the predominant conformer shown in the figures.

The AAF-G5-imino proton is observable at 25 °C (Figure B in the Supplementary Material), which suggests shielding of this proton from exchange with solvent. The AAF-G5-imino proton is transiently hydrogen bonded to an oxygen of the phosphodiester group connecting A3 and C4, as shown in Figure 10 in the 60-ps structure. In this structure the AAF-G5-imino proton is close (2.68 Å) to the A3-H3′ proton. At other times one of the AAF-G5 amino protons is transiently hydrogen bonded to a phosphate oxygen.

The location of the G5 base in the major groove is illustrated by the structures shown in Figures 8 and 10. The location of the fluorene ring is also of interest. Figure 11 provides a comparison of the overlap of the fluorene ring with the adjacent bases in the energy-minimized structure (K9DE) and in two representative structures from the molecular dynamics trajectory. Stacking interactions are clearly important in stabilizing these structures, and thus we expect the local structure to depend on the sequence surrounding the modified guanine. The recent work of Fuchs and co-workers (Belguise-Valladier & Fuchs, 1991) provides evidence that the local structure surrounding an AAF-modified guanine depends on sequence, consistent with the sequence dependence of frame-shift mutations observed in the *Nar*I sequence (Burnouf et al., 1989; Koehl et al., 1989).

Previous experiments have suggested the presence of a flexible hinge or hinge joint (Schwartz et al., 1989; Leng, 1990) at the site of the bound AAF moiety in DNA oligomers, as opposed to a fixed bend. The molecular dynamics trajectory of the hydrated AAF-9-mer exhibits further bending in the helix axis from the energy-minimized starting conformation, suggestive of a hinge-like flexibility. However, a 210-ps simulation is orders of magnitude shorter than would be required to fully simulate the motions of flexible hinges or transitions between different conformers. The major and minor conformers of the AAF-9-mer interchange with lifetimes

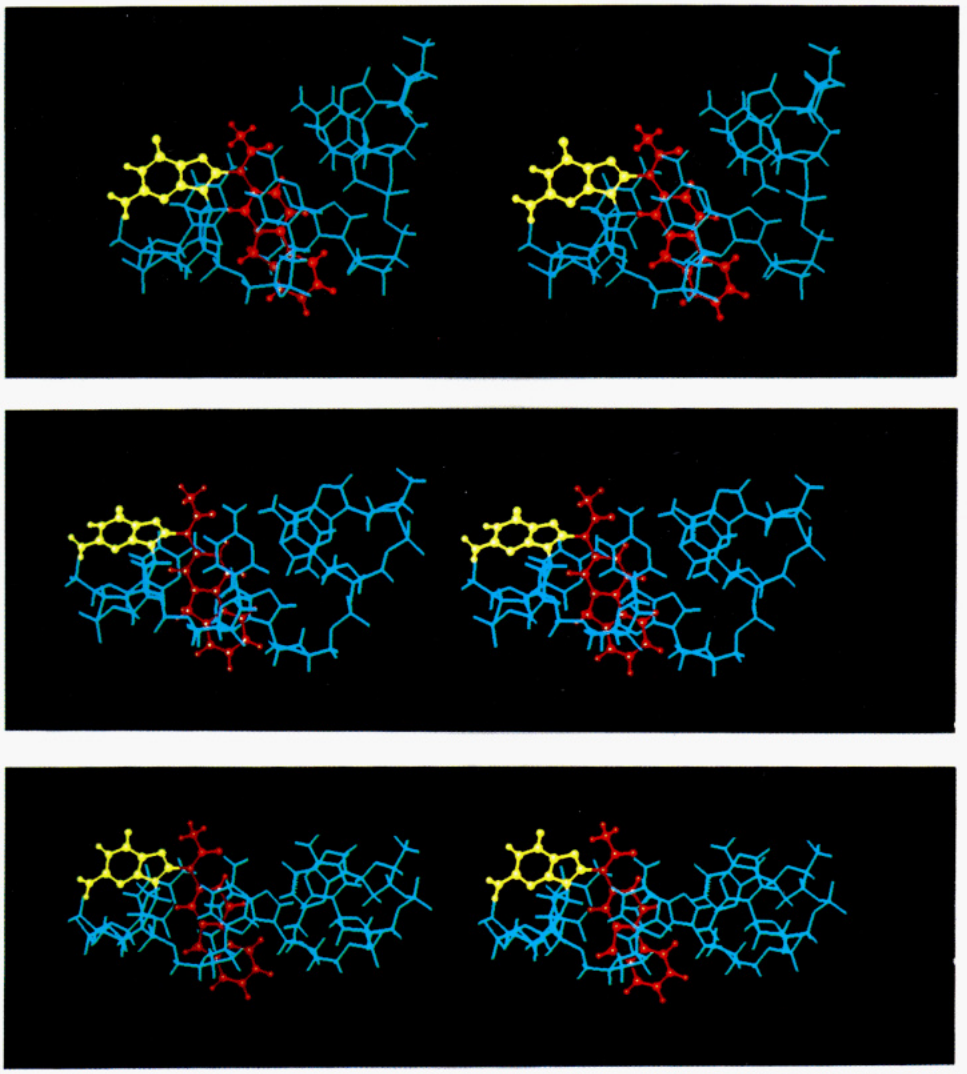

FIGURE 11: Stereoviews of the overlap of the fluorene moiety with the adjacent base pairs in (top) K9DE, (middle) K9DE60, and (bottom) K9DE160. The fluorene moiety is shown in red, the AAF-G5 base is yellow, and the remaining atoms are blue.

more than six orders of magnitude longer than the simulation. Although the motions observed in the molecular dynamics simulation are consistent with the concept of a flexible hinge, subnanosecond simulations are far too short to model chemical exchange processes observed in an NMR spectrum.

Patel and co-workers (Norman et al., 1989) studied a related molecule, 2-aminofluorene, AF. An AF-modified guanine was incorporated into a DNA 11-mer with adenine opposite the modified guanine. The AF-G base adopts a syn conformation while the A opposite the modified guanine is in the anti conformation. The aminofluorene moiety in the AF-11-mer is in the minor groove and the aminofluorene ring does not overlap with the aromatic rings of the adjacent base pairs. The aminofluorene moiety is positioned between the two strands that compose the minor groove with little distortion to the DNA duplex other than rotation of the modified guanine to syn. The present AAF structure, on the other hand, is more perturbed due to the insertion of a portion of the fluorene ring between adjacent base pairs, with attendant loss of hydrogen bonding between AAF-G5 and C14. Furthermore, the AF-11-mer with adenine opposite the modified guanine exhibited a pH dependence in structure below neutral pH, so that an unusual hydrogen bond between N1 protonated adenine and O6 of the AF-modified guanine was suggested. Even at neutral pH the N1 and O6 are essentially poised to pair. This contrasts with the present structural data on the AAF-9-mer where no pH dependence (from pH 6.0 to 8.5) was found.

The structure of another aromatic amine, 4-aminobiphenyl, bound at a guanine C^8 adopts a totally different conformation (Cho et al., 1992). In the predominant conformation of this adduct, the modified guanine adopts the anti conformation and the 4-aminobiphenyl resides in the major groove, as had been previously predicted (Broyde et al., 1985).

Several other bulky adducts that reside in the B-DNA minor groove have also been characterized. Anthramycin forms a covalent bond to the guanine 2-amino in the minor groove with little distortion to the duplex (Krugh et al., 1989). *anti*-benzo[*a*]pyrenediol epoxide also binds covalently to the same site. Patel and co-workers have recently reported the structure of both the (+)-*trans-anti*-benzo[*a*]pyrene (Cosman et al., 1992) and the (–)-*trans-anti*-benzo[*a*]pyrene (de los Santos et al., 1992) adducts bound to DNA oligomers; they found that in the (+) stereoisomer the benzo[*a*]pyrene ring long axis is oriented towards the 5′-end of the modified strand while the mirror image (–) stereoisomer has the benzo[*a*]pyrene ring oriented toward the 3′-end of the modified strand. The anthramycin and benzo[*a*]pyrene adducts involve covalent attachment at guanine N^2, and these adducts reside in the minor groove without rotation of the glycosidic torsion from the normal anti domain of B-DNA. For AAF- and AF-modified duplexes, modification is at guanine C^8 and the glycosidic torsion must rotate to syn in order to place the adduct in the minor groove.

Concluding Remarks. The analysis of the present NMR data was complicated by chemical exchange cross peaks, indicative of the presence of more than one structure, although one structure predominates in aqueous solution (≥70%). Chemical exchange cross peaks were observed over the entire temperature range used to record NOESY spectra (5–32 °C) and after the addition of magnesium ions. However, the NMR data clearly characterize the important features of the predominant conformer. The modified G5 base is in the major groove, and the fluorene ring is stacked on the C4·G15 base pair and protrudes into the minor groove as shown in Figures 8, 10, and 11. Extensive searches have been carried out in an effort to define a minor structure, and a reasonable candidate has been delineated (O'Handley, 1991). While the presence of more than one conformation of the AAF-9-mer reduces the certainty with which one may define the structure (or structures) of the adducts, it may provide important information on the range of conformations available. The ability of the AAF moiety to adopt sequence dependent and time dependent conformations may well be an important aspect of replication fidelity and lesion repair.

ACKNOWLEDGMENT

We thank Professors Robert Shapiro and Nicholas Geacintov, Chemistry Department, New York University, and Mr. Guanjin Huang, Chemistry Department, University of Rochester, for many helpful discussions.

SUPPLEMENTARY MATERIAL AVAILABLE

Figures showing the partial charges used for AAF-G5 in the AMBER simulations (Figure A), the imino proton region of the ^{1}H NMR spectrum of the AAF-9-mer as a function of temperature (Figure B), the C-H5 to C-H6 and T-CH3 to T-H6 cross peaks in the TOCSY spectrum recorded in D_2O at 32 °C (Figure C), the base to H2′/H2″ region of the NOESY spectrum recorded in D_2O at 32 °C (Figure D), the base to H3′ region of the NOESY spectrum recorded in D_2O at 32 °C with a mixing time of 450 ms (Figure E), the H1′ to H2′/H2″ region of the DQCOSY spectrum recorded in D_2O at 32 °C (Figure F), the root-mean-square deviation of the AAF-9-mer compared to the starting conformation during the molecular dynamics simulation (Figure G), and a plot of the internuclear separation of the AAF-G5-imino and A3-H3′ protons during the molecular dynamics simulation (Figure H) (15 pages). Ordering information is given on any current masthead page.

REFERENCES

Basu, A. K., & Essigmann, J. M. (1988) *Chem. Res. Toxicol. 1*, 1–18.

Beland, F. A., & Kadlubar, F. F. (1990) Metabolic Activation and DNA Adducts of Aromatic Amines and Nitroaromatic Hydrocarbons, *Handbook of Experimental Pharmacology: Chemical Carcinogenesis and Mutagenesis*, pp 267–325, Springer Verlag, Heidelberg.

Belguise-Valladier, P., & Fuchs, R. P. P. (1991) *Biochemistry 30*, 10091–10100.

Beveridge, D. L., Swaminathan, S., Ravishanker, G., Withka, J. M., Srinivasan, J., Prevost, C., Louise-May, S., Langlley, D. R., DiCapua, F. M., & Bolton, P. H. (1993) Molecular Dynamics Simulations on the Hydration, Structure and Motions of DNA Oligomers, *Top. Mol. Struct. Biol. 17* in press.

Bichara, M., & Fuchs, R. P. P. (1985) *J. Mol. Biol. 183*, 341–351.

Broyde, S., & Hingerty, B. E. (1987) *Nucleic Acids Res. 15*, 6539–6552.

Broyde, S., Hingerty, B. E., & Srinivasan, C. (1985) *Carcinogenesis 6*, 719–725.

Broyde, S., Hingerty, B. E., Shapiro, R., & Norman, D. (1990) Unusual Hydrogen Bonding Patterns in 2-Aminofluorene (AF) and 2-Acetylaminofluorene (AAF) Modified DNA, *Nitroarenes. Occurrence, Metabolism, and Biological Impact, pp 113–123, Plenum Press, New York and London.*

Burnouf, D., Koehl, P., & Fuchs, R. P. (1989) *Proc. Natl. Acad. Sci. U.S.A. 86*, 4147–4151.

Cho, B. P., Beland, F. A., & Marques, M. M. (1992) *Biochemistry 31*, 9587–9602.

Cosman, M., de los Santos, C., Fiala, R., Hingerty, B. E., Singh, S. B., Ibanez, V., Margulis, L. A., Live, D., Geacintov, N. E., Broyde, S., & Patel, D. J. (1992) *Proc. Natl. Acad. Sci. U.S.A. 89*, 1914–1918.

Evans, F. E., & Levine, R. A. (1987) *Biopolymers 26*, 1035–1046.

Evans, F. E., & Levine, R. A. (1988) *Biochemistry 27*, 3046–3055.

Evans, F. E., Miller, D. W., & Beland, F. A. (1980) *Carcinogenesis 1*, 955–959.

Fritsch, V., & Westhof, E. (1991) *J. Comput. Chem. 12*, 147–166.

Fuchs, R. P. P., & Daune, M. (1971) *FEBS Lett 14*, 206–208.

Fuchs, R. P. P., & Daune, M. (1972) *Biochemistry 11*, 2659–2666.

Gronenborn, A. M., & Clore, G. M. (1985) *Investigation of the Solution Structures of Short Nucleic Acid Fragments by Means of Nuuclear Overhauser Enhancement Measurements*, Pergamon Press, Great Britain.

Grunberger, D., Nelson, J. H., Cantor, C. R., & Weinstein, I. B. (1970) *Proc. Natl. Acad. Sci. U.S.A. 66*, 488–494.

Hausheer, F. M., Singh, U. C., Saxe, J. D., & Colvin, D. M. (1989) *Anticancer Drug Des. 4*, 281–294.

Hingerty, B. E., & Broyde, S. (1982a) *Biochemistry 21*, 3243–3252.

Hingerty, B. E., & Broyde, S. (1982b) *Int. J. Quant. Chem. 9*, 125–136.

Hingerty, B. E., Figueroa, T. L. H., & Broyde, S. (1989) *Biopolymers 28*, 1195–1222.

Huang, G., & Krugh, T. R. (1990) *Anal. Biochem. 190*, 21–25.

Jorgensen, W. L., Chandrasekhar, J., Madura, J. D., Impey, R. W., & Klein, M. L. (1983) *J. Chem. Phys. 79*, 926–935.

Kan, L. S., Cheng, D. M., Jayaraman, K., Leutzinger, E. E., Miller, P. S., & Ts'o, P. O. P. (1982) *Biochemistry 21*, 6723–6732.

Koehl, P., Valladier, P., Lefevre, J.-F., & Fuchs, R. P. P. (1989) *Nucleic Acids Res. 17*, 9531–9541.

Kriek, E. (1969) *Chem.-Biol. Interact. 1*, 3–17.

Krugh, T. R., Graves, D. E., & Stone, M. P. (1989) *Biochemistry 28*, 9988–9994.

Lambert, I. B., Napolitano, R. L., & Fuchs, R. P. P. (1992) *Proc. Natl. Acad. Sci. U.S.A. 89*, 1310–1314.

Leng, M. (1990) *Biophys. Chem. 35*, 155–163.

Leng, M., Ptak, M., & Rio, P. (1980) *Biochem. Biophys. Res. Commum. 96*, 1095–1102.

Lipkowitz, K. E., Chevalier, T., Widdifield, M., & Beland, F. A. (1982) *Chem.-Biol. Interact. 40*, 57–76.

Nelson, J. H., Grunberger, D., Cantor, C. R., & Weinstein, I. B. (1971) *J. Mol. Biol 62*, 331–346.

Nerdal, W., Hare, D. R., & Reid, B. R. (1988) *J. Mol. Biol 201*, 717–739.

Nikonowicz, E. P., Meadows, R. P., Fagan, P., & Gorenstein, D. G. (1991) *Biochemistry 30*, 1323–1334.

Norman, D., Abuaf, P., Hingerty, B. E., Live, D., Grunberger, D., Broyde, S., & Patel, D. (1989) *Biochemistry 28*, 7462–7476.

O'Handley, S. F. (1991) Ph.D. Thesis, Structural Analysis of a Carcinogen-Modified DNA Oligomer by NMR Spectroscopy, University of Rochester, Rochester, NY.

O'Handley, S. F., Sanford, D. G., Xu, R., Lester, C. C., Hingerty, B. E., Broyde, S., & Krugh, T. R. (1992) Structure of a Acetylaminofluorene (AAF) Modified DNA Oligomer, *Structure and Function, Volume I: Nucleic Acids*, pp 137–145, Adenine Press, NY.

Pardi, A., Walker, R., Rapoport, H., Wider, G., & Wuthrich, K. (1983) *J. Am. Chem. Soc. 105*, 1652–1653.

Patel, D. J., & Shapiro, L. (1985) *Biochimie 67*, 887–915.

Powers, R., Olsen, R. K., & Gorenstein, D. G. (1989) *J. Biomol. Struct. Dyn. 7*, 515–556.

Sage, E., & Leng, M. (1980) *Proc. Natl. Acad. Sci. U.S.A. 77*, 4597–4601.

Sanford, D. G. (1986) Ph.D. Thesis, Physical Studies of the Covalent Adduct of *N*-Acetoxy-2-Acetylaminofluorene with DNA, University of Rochester, Rochester, NY.

Sanford, D. G., &Krugh, T. R. (1985) *Nucleic Acids Res. 13*, 5907–5917.

Santella, R. M., Grunberger, D., Broyde, S., & Hingerty, B. E. (1981a) Nucleic Acids Res. 9, 5459–5467.

Santella, R. M., Grunberger, D., Weinstein, I. B., & Rich, A. (1981b) *Proc. Natl. Acad. Sci. U.S.A. 78*, 1451–1455.

Schlick, T., Hingerty, B. E., Peskin, C. S., Overton, M. L., & Broyde, S. (1990) *Theoretical Chemistry and Molecular Biophysics*, Academic Press, New York.

Schmitz, U., Zon, G., & James, T. L. (1990) *Biochemistry 29*, 2357–2368.

Schwartz, A., Marrot, L., & Leng, M. (1989) *J. Mol. Biol 207*, 445–450.

Shapiro, R., Hingerty, B. E., & Broyde, S. (1989) *J. Biomol. Struct. Dyn. 7*, 493–513.

Sharma, M., & Box, H. C. (1985) *Chem.-Biol. Interact. 56*, 73–88.

Singer, B., & Grunberger, D. (1983) *Molecular Biology of Mutagens and Carcinogens, Plenum, New York.*

Singh, U. C., & Kollman, P. A. (1984) *J. Comput. Chem. 5*, 129–145.

Singh, U. C., Weiner, P. K., Caldwell, J., & Kollman, P. C. (1988) *AMBER Version 3.1*, University of California, San Francisco, CA.

Srinivasan, A. R., & Olson, W. (1980) *Fed. Proc. 39*, 2199.

Taylor, E. R., & Olson, W. K. (1983) *Biopolymers 22*, 2667–2702.

van de Ven, F. J. M., & Hilbers, C. W. (1988) *Eur. J. Biochem. 178*, 1–38.

van Gunsteren, W. F., & Berendsen, H. J. C. (1977) *Mol. Phys. 34*, 1311–1327.

Veaute, X., & Fuchs, R. P. P. (1991) *Nucleic Acids Res. 19*, 5603–5606.

Wang, A. H.-J., Quigley, G. J., Kolpak, F. J., Crawford, J. L., van Boom, J. H., van der Marel, G., & Rich, A. (1979) *Nature 282*, 680–686.

Weiner, S. J., Kollman, P. A., Case, D. A., Singh, U. C., Ghio, C., Alagona, G., Profeta, S., Jr., & Weiner, P. (1984) *J. Am. Chem. Soc. 106*, 765–784.

Weiner, S. J., Kollman, P. A., Nguyen, D. J., & Case, D. A. (1986) *J. Comput. Chem. 7*, 230–252.

Withka, J. M., Swaminathan, S., Srinivasan, J., Beveridge, D. L., & Bolton, P. H. (1992) *Science 255*, 597–599.

Zhou, N., Manogaran, S., Zon, G., & James, T. L. (1988) *Biochemistry 27*, 6013–6020.